Longitudinal dynamics of clonal hematopoiesis identifies gene-specific fitness effects

nature medicine

ARTICLES

https://doi.org/10.1038/s41591-022-01883-3

Check for updates

OPEN

Longitudinal dynamics of clonal hematopoiesis identifies gene-specific fitness effects

Neil A. Robertson[1,9], Eric Latorre-Crespo[1,9], Maria Terradas-Terradas[2,3], Jorge Lemos-Portela[4], Alison C. Purcell[2,3], Benjamin J. Livesey[1], Robert F. Hillary[5], Lee Murphy[6], Angie Fawkes[6], Louise MacGillivray[6], Mhairi Copland[7], Riccardo E. Marioni[5], Joseph A. Marsh[1], Sarah E. Harris[8], Simon R. Cox[8], Ian J. Deary[8], Linus J. Schumacher[4,9] ✉, Kristina Kirschner[2,3,9] ✉ and Tamir Chandra[1,9] ✉

Clonal hematopoiesis of indeterminate potential (CHIP) increases rapidly in prevalence beyond age 60 and has been associated with increased risk for malignancy, heart disease and ischemic stroke. CHIP is driven by somatic mutations in hematopoietic stem and progenitor cells (HSPCs). Because mutations in HSPCs often drive leukemia, we hypothesized that HSPC fitness substantially contributes to transformation from CHIP to leukemia. HSPC fitness is defined as the proliferative advantage over cells carrying no or only neutral mutations. If mutations in different genes lead to distinct fitness advantages, this could enable patient stratification. We quantified the fitness effects of mutations over 12 years in older age using longitudinal sequencing and developed a filtering method that considers individual mutational context alongside mutation co-occurrence to quantify the growth potential of variants within individuals. We found that gene-specific fitness differences can outweigh inter-individual variation and, therefore, could form the basis for personalized clinical management.

Age is the single largest factor underlying the onset of many cancers[1]. Age-related accumulation and clonal expansion of cancer-associated somatic mutations in healthy tissues has been posited recently as a pre-malignant status consistent with the multi-stage model of carcinogenesis[2]. However, the widespread presence of cancer-associated mutations in healthy tissues highlights the complexity of early detection and diagnosis of cancer[3–7].

CHIP is defined as the clonal expansion of HSPCs in healthy aged individuals. CHIP affects more than 10% of individuals over the age of 60 years and is associated with an estimated ten-fold increased risk for the later onset of hematological neoplasms[3–5]. There is a clear benefit of detecting CHIP early for close clinical monitoring and early detection, as the association between clone size and malignancy progression is well-established[5,8,9].

The particular mechanisms by which common mutations of CHIP—for example, *DNMT3A* and *TET2*—contribute to the progression of leukemia are still not understood, which hinders early diagnosis of CHIP on a gene or variant basis[8,10–12]. In clinical practice, CHIP is diagnosed by the presence of somatic mutations at variant allele frequencies (VAFs) of at least 2% in cancer-associated genes, that is in more than 4% of all blood cells[8,13]. Clonal fitness, defined as the proliferative advantage of stem cells carrying a mutation over cells carrying no or only neutral mutations, has emerged as an alternative clone-specific quantitative marker of CHIP[14,15]. As mutations in stem cells often drive leukemia[5], we hypothesized that stem cell fitness contributes substantially to transformation from CHIP to leukemia.

Stratification of individuals to inform close clinical monitoring for early detection or prevention of leukemia in the future will depend on the ability to accurately associate genes and their variants with progression to disease. However, it remains unresolved whether variant-specific or gene-specific fitness effects outweigh other factors contributing to variable progression among individuals, such as environment or genetics.

Hitherto, fitness effects have been predicted from large cross-sectional cohort data[14,16]. In this approach, single-timepoint data from many individuals are pooled to generate allele frequency distributions. Although this method allows the study of a large collection of variants, pooling prevents estimation of an individual's mutational fitness effects from cross-sectional data. Inferring fitness from a single timepoint creates additional uncertainty about whether a mutation has arisen recently and has grown rapidly (high fitness advantage) or arose a long time ago and has grown slowly (low fitness advantage). With longitudinal samples, fitness effects of individual mutations can be estimated directly from the change in VAF over multiple timepoints.

In this study, we worked with longitudinal data from the Lothian Birth Cohort of 1921 (LBC1921) and the Lothian Birth Cohort of 1936 (LBC1936)[17]. Such longitudinal data are rare worldwide owing to their participants' older age (70–90 years) and their three-yearly follow-ups over 12 years in each cohort and over 21 years of total timespan. We developed a new framework for extracting fitness effects from longitudinal data using Bayesian inference. First, a

[1]MRC Human Genetics Unit, University of Edinburgh, Edinburgh, UK. [2]Institute of Cancer Sciences, College of Medical, Veterinary and Life Sciences, University of Glasgow, Glasgow, UK. [3]Cancer Research UK Beatson Institute, Glasgow, UK. [4]Centre for Regenerative Medicine, Institute for Regeneration and Repair, University of Edinburgh, Edinburgh, UK. [5]Centre for Genomic and Experimental Medicine, Institute of Genetics and Cancer, University of Edinburgh, Edinburgh, UK. [6]Edinburgh Clinical Research Facility, University of Edinburgh, Edinburgh, UK. [7]Paul O'Gorman Leukaemia Research Centre, Institute of Cancer Sciences, College of Medical, Veterinary and Life Sciences, University of Glasgow, Glasgow, UK. [8]Lothian Birth Cohorts, Department of Psychology, University of Edinburgh, Edinburgh, UK. [9]These authors contributed equally: Neil A. Robertson, Eric Latorre-Crespo, Linus J. Schumacher, Kristina Kirschner, Tamir Chandra. ✉e-mail: linus.schumacher@ed.ac.uk; kristina.kirschner@glasgow.ac.uk; tamir.chandra@igmm.ed.ac.uk

likelihood-based filter for time series data (LiFT) allowed us to segregate between sequencing artifacts or naturally drifting populations of cells and fast-growing clones. Second, we inferred the growth potential or fitness effects simultaneously for all growing mutations within each individual and also allowed for clones with multiple mutations if these are favored by Bayesian model comparison. We detected gene-specific fitness effects within our cohorts, highlighting the potential for personalized clinical management.

Results

Longitudinal profiling of CHIP variants in advanced age. The Lothian Birth Cohorts (LBCs) of 1921 ($n=550$) and 1936 ($n=1091$) are two independent, longitudinal studies of aging with approximately three-yearly follow-up for five waves, from the age of 70 years (LBC1936) and 79 years (LBC1921)[17]. We previously identified 73 participants with CHIP at wave 1 through whole-genome sequencing (WGS)[18]. Here, we used a targeted error-corrected sequencing approach using a 75-gene panel (ArcherDX/Invitae) to assess longitudinal changes in VAFs and clonal evolution over 21 years across both LBC cohorts (6 years in LBC1921 and 12 years in LBC1936; Supplementary Table 1). Error-corrected sequencing allowed accurate quantification, providing more sensitive clonal outgrowth estimates than our previous WGS data. We sequenced 248 LBC samples (85 individuals across 2–5 timepoints) and achieved a sequencing depth of 2,238× mean coverage (2,153× median) over all targeted sites with an average of 1.6 unique somatic variants (pan-cohort VAF 0.03–87%, median VAF 4.4%) detected per participant. We examined all participant-matched events across the time course: sequence quality control metrics revealed that only seven of 275 data points failed to meet our quality criteria, likely due to low initial VAF. Most of our variant loci generally displayed a high number of supporting reads, with a mean of 258 (Extended Data Fig. 1a).

For our initial analysis, we retained variants with at least one timepoint at 2% VAF (Supplementary Table 2). *DNMT3A* was the most commonly mutated CHIP gene ($n=39$ events in 33 participants), followed by *TET2* ($n=18$ events in 15 participants), *JAK2* ($n=8$ events in eight participants) and *ASXL1* ($n=3$ events in three participants) (Fig. 1a–c and Extended Data Fig. 1e). Our mutation spectrum is consistent with previous studies in finding *DNMT3A* and *TET2* as the most frequently mutated genes[4,5]. We detected some variants more frequently at certain hotspots within a gene, such as R882H in *DNMT3A*, with previously unreported variants being present as well (Fig. 1d–i and Supplementary Table 2)[5]. We most frequently detected missense mutations with several other key protein-altering event types ranking highly, including frameshift insertions and deletions and nonsense mutations (Fig. 1a–c). Participants broadly cluster together across their time course, driven by the expanding or stable VAF of their harbored mutations, underscoring the high prevalence and large clone size of common clonal hematopoietic drivers, namely *DNMT3A*, *TET2* and *JAK2* (Fig. 1a–c). In the case of *JAK2V617F*, we identified two individuals who developed leukemia at wave 2 and received treatment between waves 2 and 3, likely driving a clear reduction in clone size (Fig. 1h). Those individuals were excluded from further analysis. In our data, we identified a lower frequency of mutations in splicing genes, such as *SF3B1*, despite the older age of the cohorts (Fig. 1a and Extended Data Fig. 1e). This is in contrast to previously published cohort data, where splicing mutations became more prominent with increased age[19]. Most mutations were missense, frameshift and nonsense mutations (Fig. 1b).

Overall, our sequencing approach allowed for high-resolution, longitudinal mapping of CHIP variants over 6-year and 12-year time spans in LBC1921 and LBC1936, respectively, and 21-year time span across both cohorts from the same geographical region and born 9 years apart.

Cataloguing of fitness effects for CHIP variants at >2% VAF. Stem cell fitness is defined as the proliferative advantage over cells carrying no or only neutral mutations. It remains incompletely understood to what extent fitness is gene-specific or variant-specific or determined by the bone marrow microenvironment and clonal composition. Earlier estimates suggested a wide spread of fitness effects even for variants of the same gene[14], which would make it difficult to clinically stratify individuals with CHIP. To determine the fitness effects of the variants identified in our cohorts (Fig. 1a and Extended Data Fig. 1e), we initially selected all CHIP variants in our data using the commonly used criterion of defining any variants with VAF > 2% as CHIP[8,13] and retaining only those variants with at least two timepoints (Fig. 2b). This approach identified 76 CHIP mutations overall (Fig. 2c). To estimate the fitness effect that each variant confers, we used Bayesian inference and birth–death models of clonal dynamics (Fig. 2a), including all trajectories with at least two timepoints (Supplementary Table 3). The resulting fitness values show an overall dependence of fitness on the gene level (Fig. 2d), with a wide distribution of fitness for some genes, such as *TET2* and *DNMT3A*, but not others, such as *JAK2* (which are all the same variant).

Longitudinal trajectories accurately stratify CHIP variants. Because longitudinal data allow direct quantification of the growth in VAF over time, we can inspect the gradients (fluctuations) in VAF for variants that were classified as CHIP based on thresholding. We found that a VAF > 2% threshold not only misses fast-growing and potentially harmful variants (Fig. 2b) but can also include variants whose frequencies are shrinking (Fig. 2b,c) and, thus, either do not confer a fitness advantage or are being outcompeted by other clones. Overall, 70% of CHIP mutations detected by thresholding at 2% VAF were growing during the observed time span (Fig. 2b,c). Longitudinal data, thus, reveal limitations in defining CHIP mutations based on a widely used VAF threshold.

Fig. 1 | Clonal hematopoiesis in the LBCs. a, Counts of unique events that exceeded 2% VAF across the range of the longitudinal cohorts in our panel of 75 hematopoietic genes. **b**, Counts of the functional consequences of the unique events listed in Fig. 1a. Missense mutations, frameshift insertions and deletions and nonsense mutations are indicated. Exact counts, *n*, are for each category. **c**, Schematic of the top seven most affected genes in the cohort with the largest clone size of an event in any given gene shown. All affected participants were clustered across all timepoints, with the point size scaled by VAF and colored by the functional consequence of the variant (as per Fig. 1b and legend). **d**, Clone size trajectories of all *DNMT3A* mutations across the time series in both LBC1921 and LBC1936 colored by the functional consequence of the variant (as per Fig. 1b,c). **e**, Locations of somatic mutations discovered in *DNMT3A*. Protein-affecting events are marked and labeled across the structure of the gene (missense in red, truncating in purple, stacked for multiple events) with the structure of the gene labeled along the amino acid length of its protein. **f**. Clone size trajectories of all *TET2* mutations across the time series in both LBC1921 and LBC1936 colored by the functional consequence of the variant (as per Fig. 1b,c). **g**, The locations of somatic mutations in *TET2*. Protein-affecting events are marked and labeled across the structure of the protein (missense in red, truncating in purple, stacked for multiple events). **h**, Clone size trajectories of all *JAK2* mutations across the time series in both LBC1921 and LBC1936 colored by the functional consequence of the variant (as per Fig. 1b,c). Points marked in black denote timepoints after which the affected participant received treatment for leukemia. **i**, The locations of somatic mutations in *JAK2*. Protein-affecting events are marked and labeled across the structure of the protein (missense in red, truncating in purple, stacked for multiple events). All eight *JAK2* mutations are p.Val617Phe (*JAK2 V617F*) missense variants. del, deltion; FS, frameshift; ins, insertion.

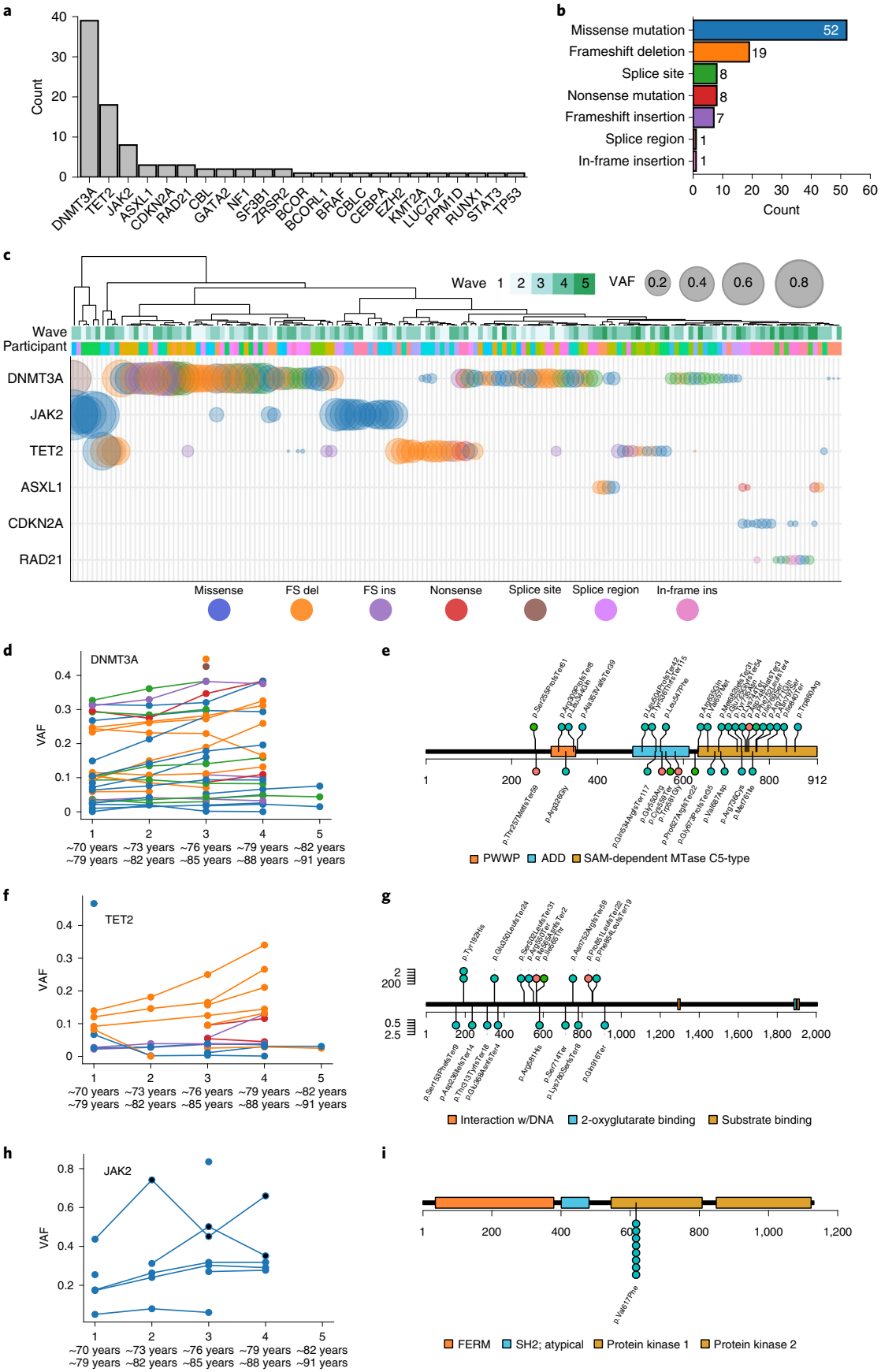
a
Count
DNMT3A TET2 JAK2 ASXL1 CDKN2A RAD21 CBL GATA2 NF1 SF3B1 ZRSP2 BCOR BCORL1 BRAF CBLC CEBPA EZH2 KMT2A LUC7L2 PPM1D RUNX1 STAT3 TP53
b
Missense mutation 52
Frameshift deletion 19
Splice site 8
Nonsense mutation 8
Frameshift insertion 7
Splice region 1
In-frame insertion 1
Count
c
Wave 1 2 3 4 5
VAF 0.2 0.4 0.6 0.8
Wave
Participant
DNMT3A
JAK2
TET2
ASXL1
CDKN2A
RAD21
Missense FS del FS ins Nonsense Splice site Splice region In-frame ins
d
DNMT3A
VAF
~70 years ~73 years ~76 years ~79 years ~82 years
~79 years ~82 years ~85 years ~88 years ~91 years
e
PWWP ADD SAM-dependent MTase C5-type
f
TET2
VAF
~70 years ~73 years ~76 years ~79 years ~82 years
~79 years ~82 years ~85 years ~88 years ~91 years
g
Interaction w/DNA 2-oxyglutarate binding Substrate binding
h
JAK2
VAF
~70 years ~73 years ~76 years ~79 years ~82 years
~79 years ~82 years ~85 years ~88 years ~91 years
i
FERM SH2; atypical Protein kinase 1 Protein kinase 2

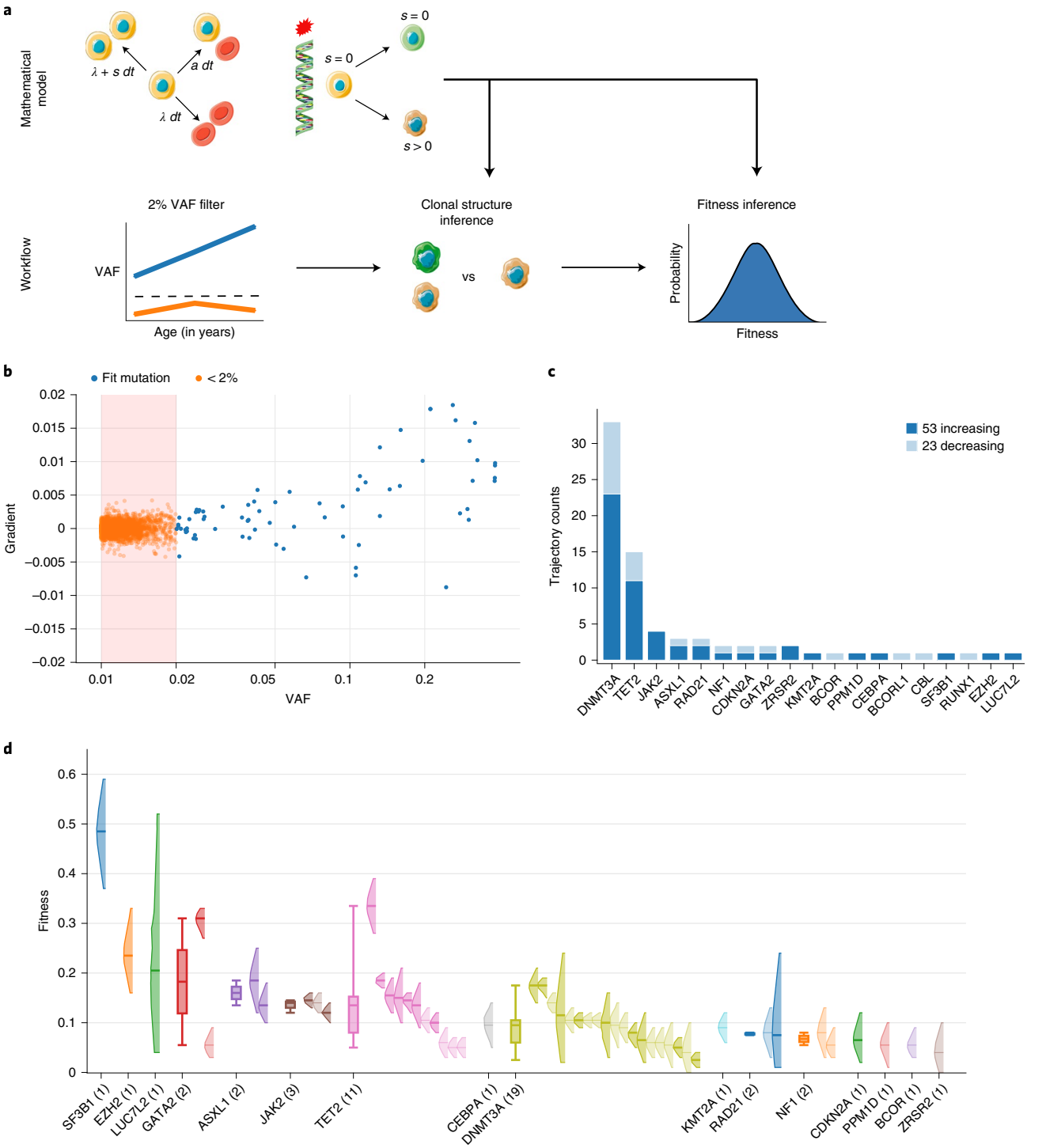

Fig. 2 | Fitness effects of variants at 2% VAF threshold in longitudinal data. a, Schematic of the mathematical model (top) and workflow (bottom) used to infer the fitness of mutations reaching VAF > 2% during the observed time span. Clonal structure and fitness inference are based on a mathematical model of clonal dynamics (Methods). HSPCs (top, yellow cells) naturally acquire mutations over time that can be neutral ($s = 0$, green cell) or increase self-renewal bias ($s > 0$, brown cell), leading to the formation of genetic clones. Artwork includes images by Servier Medical Art licensed under CC BY 3.0. **b**, VAF measurement $v(t_0)$ at initial timepoint t_0 versus gradient in VAF, $(v(t_{end}) - v(t_0))/(t_{end} - t_0)$, between initial and last timepoints t_0 and t_{end} of all variants detected in the LBCs with at least two timepoints. Each data point corresponds to a trajectory in the LBCs and has been colored according to its CHIP status based on the 2% VAF threshold (red box). Blue and orange, respectively, denote whether trajectories achieved a VAF > 2% during the observed time span or not. Note: VAF is displayed on a logarithmic scale, as most mutations are concentrated at low VAF. **c**, Number of trajectories passing the currently used 2% VAF threshold, broken down into whether VAF is increasing or decreasing from the first to last timepoint. **d**, Fitness effects of mutations grouped by gene and ranked by median fitness. The posterior probability distribution of the fitness as inferred from our model of clonal dynamics is displayed for each mutation (only the 90% interval is shown). The sample size, *n*, of observed variants in each gene is denoted in brackets. When more than one mutation is observed in a gene, we further display a box plot showing the median and exclusive interquartile range of the MAP fitness estimates associated with the gene.

To overcome the limitations of a threshold-based selection of fit variants, we sought to filter variants based on longitudinal information, by comparing a stochastic model of clonal dynamics with a model of sequencing artifacts (Fig. 3a). This novel approach, which we named LiFT, allows classification of fit variants even for VAF < 2%. LiFT classification of fit variants broadly agreed with noise profile statistics from the ArcherDX pipeline (Extended Data Fig. 2f,g) but identified additional variants by leveraging the longitudinal nature of the data. LiFT classification resulted in 114 variant trajectories (Fig. 3b–d and Extended Data Fig. 2a–g), 86% of which grew over the observed time span. We note that the VAF of fit mutations may still shrink over time due to the presence of an even fitter clone in the same individual. This is in contrast to thresholding at 2% VAF, with only 70% of variants identified to be growing and, thus, likely to confer a fitness advantage. Of the 114 variants we detected, 50 would not have been detected using the previous VAF threshold filter. We, therefore, recomputed fitness estimates for this new set of fit trajectories (Fig. 3e,f). Growing variants that were missed by the traditional filtering method include highly fit variants such as *U2AF1* Q157R (fitness 33.5%) and *DNMT3A* R882H (fitness 16%) (Fig. 3c,g and Supplementary Table 4). VAF thresholding did not identify any *TP53* variants. However, LiFT identified four *TP53* mutations, all of which were growing over the observed time course (Fig. 3c,g and Supplementary Table 4). In addition, all of those were either termination/frameshift mutations or previously reported as cancer-associated in the Catalogue of Somatic Mutations in Cancer (COSMIC)[20] and classified as likely damaging (Supplementary Table 5). Moreover, all *TP53* variants led to high fitness effects; thus, our filtering method allows us to identify potentially harmful variants at very low VAFs. Overall, the variants detected by LiFT were of higher fitness than those detected by VAF thresholding (Fig. 3f; Kruskal–Wallis $H = 14$, $P = 1 \times 10^{-4}$), with an even larger effect size when comparing variants that are exclusive to each filtering algorithm (Fig. 3f; Kruskal–Wallis $H = 18$, $P = 1 \times 10^{-5}$).

We further stratified variants using seven computational predictors recently identified as being most useful for identifying pathogenic mutations[21–27] (Fig. 3g and Supplementary Table 5), categorizing the most prevalent CHIP variants into likely damaging (21 variants), possibly damaging (20 variants) and likely benign (11 variants) as well as frameshifts and terminations (37 variants, which are also most likely damaging to protein structure and, thus, protein function; Supplementary Table 6). Our novel LiFT algorithm, therefore, produces a low false discovery rate of pathogenic variants, with 88% of the detected fit variants being predicted to be possibly damaging, frameshift or termination.

Taken together, applying a probabilistic model of clonal dynamics to longitudinal sequencing data results in a novel method—the LiFT algorithm—that improves on the threshold-based definition of CHIP mutations (Fig. 3a). The LiFT algorithm replaces an arbitrary cutoff on VAF by a choice of false discovery rate (through a Bayes factor threshold) and, as a result, selects fewer trajectories with shrinking VAF (Figs. 2b,c and 3b–d).

Clinical relevance of LiFT. We further analyzed differences in the distributions of fitness between genes using a non-parametric test. Despite having small sample sizes for many genes, we still detected statistically significant differences among the distributions of fitness effects (Fig. 4a,b). In particular, we found that mutations in *TP53*, *SF3B1* and *SRSF2* conferred a higher fitness advantage over mutations in commonly mutated CHIP genes, such as *JAK2* and *DNMT3A*. We also tested differences in fitness by genes when summarized into functional categories and found trajectories of genes involved in DNA methylation to have lower fitness than genes involved in splicing and genes for transcription factors that are relevant in development (Extended Data Fig. 3a,b).

Differences in the distribution of fitness allow us to predict the future growth of mutations from initial timepoints. For example, if a patient presents with a variant in a gene with 10% fitness at 1% VAF, its growth could be confidently measured after 7 months (Fig. 4c), warranting a clinical follow-up over that timeframe to confirm or revise the fitness estimate. Conversely, the time between observations places a lower bound on the fitness that can be measured for mutations of a given VAF (Fig. 4d). These data can then inform on the timeframe for close clinical monitoring and early detection of disease.

Ableson et al.[16] compared CHIP carriers who never developed acute myeloid leukemia (AML) with CHIP where individuals subsequently developed AML, and they found that the number of mutations, the mutational burden and the size of the larger driver clone were associated with the risk of progression to AML. In the present study, we carried out a survival analysis to correlate the maximum observed VAF of mutations and survival. This correlation was stronger in the older cohort (LBC1921) although not statistically significant (hazard ratio (HR) = 1.35; 95% confidence interval (CI) 0.83, 2.19; $P = 0.23$) due to the small sample size (Extended Data Fig. 3d and Supplementary Table 7). In the younger cohort (LBC1936), we found that survival better correlated with the speed of growth of a mutation, although this was, again, not statistically significant (HR = 1.35; 95% CI 0.76, 2.4; $P = 0.3$) (Extended Data Fig. 3d and Supplementary Table 7).

Notably, only two timepoints are necessary to apply LiFT, making this a widely applicable method for existing cohorts and future studies (Extended Data Fig. 3c). We propose the use of LiFT over thresholding for clinical practice.

Discussion

The clinical potential for stratifying progression of CHIP depends on whether genes confer distinct fitness advantages. Indeed, most studies so far have not shown a clear distinction of fitness effects on

Fig. 3 | LiFT allows classification of fit variants <2% VAF. a, Schematic of LiFT algorithm. LiFT compares a model of clonal dynamics (Fig. 1a) with an artifact model and performs Bayesian model selection. The subsequent steps to infer clonal structure and fitness distributions are as in Fig. 1a. **b**, Gradient in VAF versus VAF for variants detected in the LBCs with at least two timepoints and at least one VAF > 1% per trajectory, with filtered (orange), fit (blue) and synonymous (light green dots) mutations, classified by LiFT on a logarithmic scale. **c**, Longitudinal trajectories of fit (blue) and filtered (orange) mutations linked to age in years. **d**, Number of trajectories classified as fit by LiFT, broken down into increasing or decreasing VAF from first to last timepoint. **e**, Left, deterministic fit of all mutations selected by LiFT in an individual of the LBC cohorts using the inferred optimal clonal structure (Supplementary Information Methods, Appendix B). 90% CIs associated with binomial sampling noise are shown for each data point. VAF is displayed on a logarithmic scale. Right, posterior distribution of fitness associated to each clonal structure. **f**, Fitness effects of variants broken down by filtering method. The sample size, *n*, and statistical analyses comparing the distribution of fitness, computed using the non-parametric Kruskal–Wallis test, are highlighted (*$H = 14$, $P = 1 \times 10^{-4}$; **$H = 18$, $P = 1 \times 10^{-5}$). **g**, Fitness of variants selected as fit by LiFT broken down by their maximum VAF, >2% and <2%, and damage prediction. The top row displays a bar plot of variant counts for each category. The bottom row displays box plots showing the median and interquartile range of the distribution of MAP fitnesses by damaging prediction displayed on a logarithmic scale to emphasize relative differences in fitness between variants. Consequently, of a total of 89 variants with a damage prediction, 17 variants with fitness below 2% are not shown but are reported in Supplementary Tables 4–6. A marginal plot shows the Gaussian kernel density estimation of the MAP fitness values. fs, frameshifts; ter, terminations.

a gene basis and have shown considerable overlap in fitness coefficients among variants of different genes. We show that fitness can substantially differ by gene and gene category. Combining longitudinal data with a new method to identify CHIP variants allows for more accurate fitness estimates of CHIP than cross-sectional cohort data and motivates further studies with increased sample sizes.

Our fitness estimates are independent of the time when the mutation was acquired. In cross-sectional studies, fitness

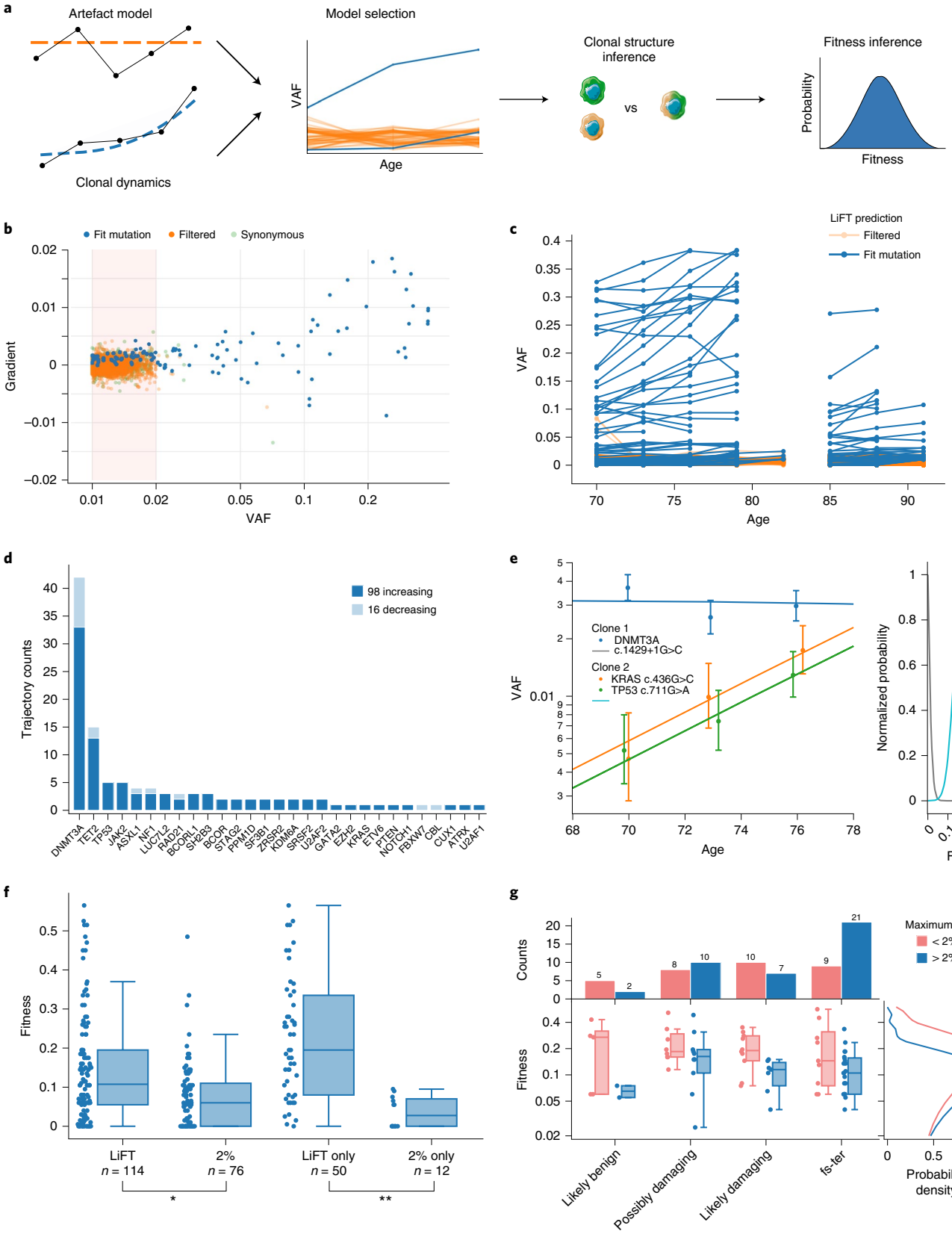

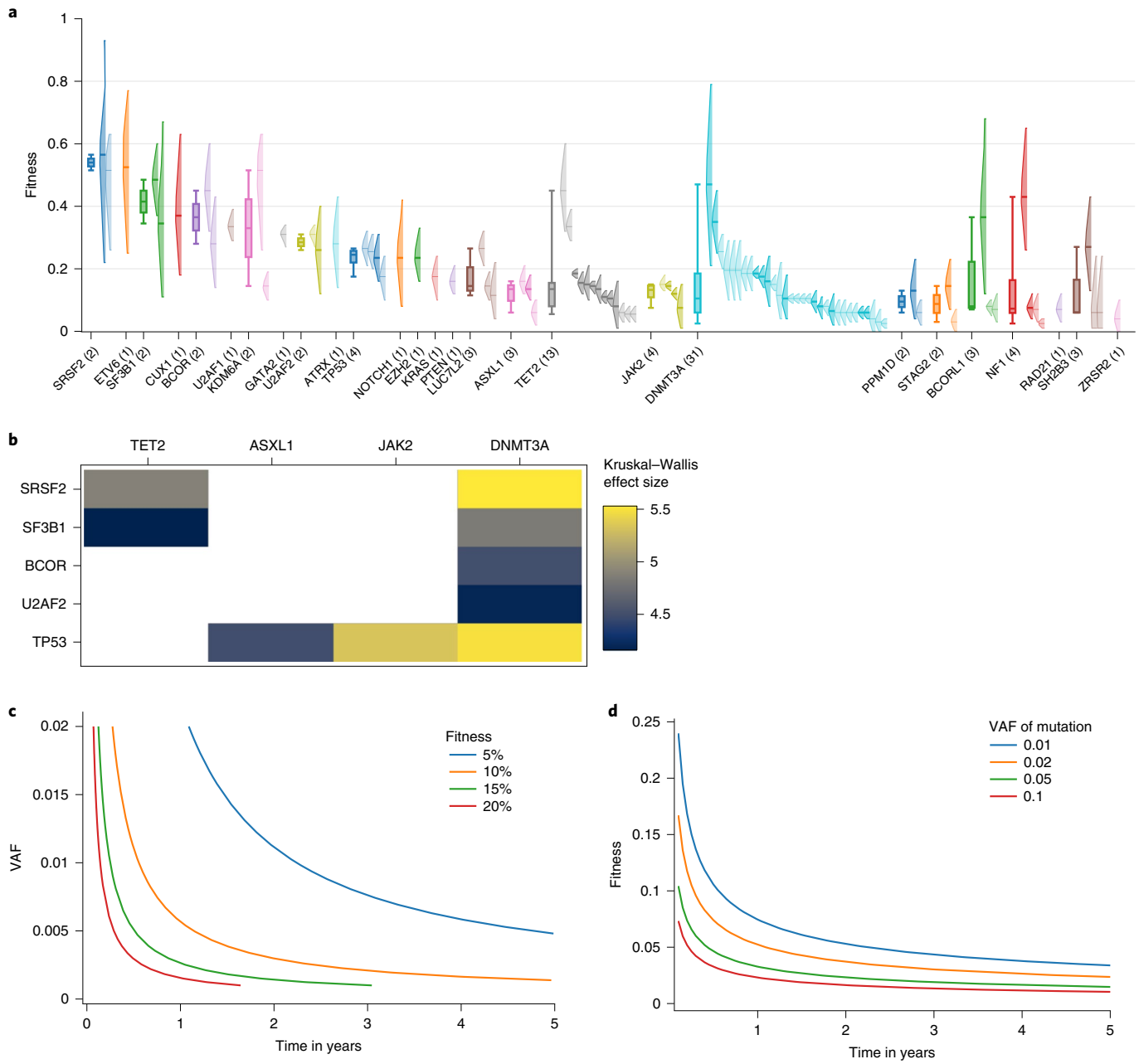

Fig. 4 | Clinical relevance of LiFT. a, Fitness effects of mutations selected as fit by the LiFT algorithm, grouped by gene and ranked by median fitness. The posterior probability distribution of the fitness as inferred from our model of clonal dynamics is displayed for each mutation (only the 90% interval is shown). The sample size, *n*, of observed variants in each gene is denoted in brackets. When more than one mutation is observed in a gene, we further display a box plot showing the median and exclusive interquartile range of the MAP estimates of fitness associated with the gene. **b**, Analysis of variance of the distribution of fitness across genes. Heat map of all statistically significant ($P < 0.05$) Kruskal–Wallis H statistics, labeled by effect size, computed for all combinations of pairs of genes. The effect size is only shown for statistically significant relations. Variants with a fitness below 2% were left out of this study, as our prediction classifies them as conferring no or a negligible fitness advantage. **c**, Minimum referral time in years based on 2 standard deviations below the expected growth of a clone given an initial VAF and fitness. Each line shows the initial size of mutation versus referral time for a given fitness. **d**, Minimum detectable fitness at referral observation based on 2 standard deviations below the expected growth of a clone given an initial VAF and fitness. Each line shows minimum detectable fitness versus referral time for an initial clone size.

estimates are generally (inversely) correlated with the mutation rate, introducing additional uncertainty[14]. In contrast, our fitness estimates are based on the observed growth among longitudinal samples and, thus, also take into account other mutations in an individual. The resulting fitness estimates are largely independent of hematopoietic stem cell absolute numbers (Extended Data Fig. 4b,c).

The strength of our approach, combining longitudinal data with our LiFT algorithm, is exemplified by *U2AF1* and *TP53*, for which no variants were identified by a 2% VAF threshold (Fig. 2b,c). In contrast, our LiFT method identified one *U2AF1* and four *TP53* variants, all of which are conferring a fitness advantage, scored as possibly damaging in our missense variant effect analysis and have been previously reported in COSMIC[20] (Fig. 3g and Supplementary

Tables 4 and 5). Moreover, we pick up the *DNMT3A R88H* variant with LiFT but not with 2% VAF thresholding—a mutation that is well-reported in the context of leukemia[28]. Therefore, for patients with those variants, close clinical monitoring for early detection of disease such as leukemia is merited.

Combining longitudinal data with LiFT enables a personalized approach managing CHIP (Extended Data Figs. 5 and 6). Longitudinal data allow quantifying fitness effects even for mutations not seen in large cohorts, as cross-sectional fitness estimation requires a mutation to be observed in multiple individuals. Our method offers clinicians a way forward for patient stratification even for unique variants occurring in single individuals, because two timepoints for one individual suffice to estimate fitness, including uncertainty quantification (Fig. 4e). We have provided a prediction of the time required between first and second observations to be able to accurately infer fitness, depending on the initial VAF of a mutation in an individual (Fig. 4c). For high fitness mutations (>10%), a follow-up clinical observation could be performed after only a few months, even for small clones (1% VAF or less). Conversely, the time between observations places a lower bound on the fitness that can be measured for mutations of a given VAF (Fig. 4d). In the future, these data can be used to inform time to the next appointment for close clinical monitoring of patients with clones containing highly fit variants, which will likely outcompete other clones. Using longitudinal data to better quantify and predict clonal progression in our study, however, comes with a tradeoff in the lower number of participants in our cohort and limits the power of cross-sectional analysis to find associations.

In addition, our inference method aims to resolve the clonal composition of multiple mutations in an individual. Specifically, we can now infer the likely co-occurrence of mutations from longitudinal data. Current cross-sectional studies do not take into account the clonal composition of individuals and, therefore, make predictions of the isolated effect of a mutation. In contrast, we are able to link fitness to clones carrying a specific combination of mutations that is unique to each individual, without relying on any prior knowledge of variant-specific fitness effects (Supplementary Table 4).

Online content

Any methods, additional references, Nature Research reporting summaries, source data, extended data, supplementary information, acknowledgements, peer review information; details of author contributions and competing interests; and statements of data and code availability are available at https://doi.org/10.1038/s41591-022-01883-3.

Received: 3 September 2021; Accepted: 27 May 2022;
Published online: 04 July 2022

References

1. de Magalhaes, J. P. How ageing processes influence cancer. *Nat. Rev. Cancer* **13**, 357–365 (2013).
2. Martincorena, I. Somatic mutation and clonal expansions in human tissues. *Genome Med.* **11**, 35 (2019).
3. Ayachi, S., Buscarlet, M. & Busque, L. 60 years of clonal hematopoiesis research: from X-chromosome inactivation studies to the identification of driver mutations. *Exp. Hematol.* **83**, 2–11 (2020).
4. Genovese, G. et al. Clonal hematopoiesis and blood-cancer risk inferred from blood DNA sequence. *N. Engl. J. Med.* **371**, 2477–2487 (2014).
5. Jaiswal, S. et al. Age-related clonal hematopoiesis associated with adverse outcomes. *N. Engl. J. Med.* **371**, 2488–2498 (2014).
6. Lee-Six, H. et al. The landscape of somatic mutation in normal colorectal epithelial cells. *Nature* **574**, 532–537 (2019).
7. Martincorena, I. et al. High burden and pervasive positive selection of somatic mutations in normal human skin. *Science* **348**, 880–886 (2015).
8. Jaiswal, S. & Ebert, B. L. Clonal hematopoiesis in human aging and disease. *Science* **366**, eaan4673 (2019).
9. Park, S. J. & Bejar, R. Clonal hematopoiesis in cancer. *Exp. Hematol.* **83**, 105–112 (2020).
10. Terradas-Terradas, M., Robertson, N. A., Chandra, T. & Kirschner, K. Clonality in haematopoietic stem cell ageing. *Mech. Ageing Dev.* **189**, 111279 (2020).
11. Challen, G. A. & Goodell, M. A. Clonal hematopoiesis: mechanisms driving dominance of stem cell clones. *Blood* **136**, 1590–1598 (2020).
12. Shih, A. H., Abdel-Wahab, O., Patel, J. P. & Levine, R. L. The role of mutations in epigenetic regulators in myeloid malignancies. *Nat. Rev. Cancer* **12**, 599–612 (2012).
13. Steensma, D. P. & Bolton, K. L. What to tell your patient with clonal hematopoiesis and why: insights from two specialized clinics. *Blood* **136**, 1623–1631 (2020).
14. Watson, C. J. et al. The evolutionary dynamics and fitness landscape of clonal hematopoiesis. *Science* **367**, 1449–1454 (2020).
15. Williams, M. J. et al. Measuring the distribution of fitness effects in somatic evolution by combining clonal dynamics with dN/dS ratios. *eLife* **9**, e48714 (2020).
16. Abelson, S. et al. Prediction of acute myeloid leukaemia risk in healthy individuals. *Nature* **559**, 400–404 (2018).
17. Taylor, A. M., Pattie, A. & Deary, I. J. Cohort profile update: the Lothian Birth Cohorts of 1921 and 1936. *Int. J. Epidemiol.* **47**, 1042–1042r (2018).
18. Robertson, N. A. et al. Age-related clonal haemopoiesis is associated with increased epigenetic age. *Curr. Biol.* **29**, R786–R787 (2019).
19. McKerrell, T. et al. Leukemia-associated somatic mutations drive distinct patterns of age-related clonal hemopoiesis. *Cell Rep.* **10**, 1239–1245 (2015).
20. Tate, J. G. et al. COSMIC: the Catalogue Of Somatic Mutations In Cancer. *Nucleic Acids Res.* **47**, D941–D947 (2019).
21. Carter, H., Douville, C., Stenson, P. D., Cooper, D. N. & Karchin, R. Identifying Mendelian disease genes with the Variant Effect Scoring Tool. *BMC Genomics* **14**, S3 (2013).
22. Hecht, M., Bromberg, Y. & Rost, B. Better prediction of functional effects for sequence variants. *BMC Genomics* **16**, S1 (2015).
23. Ioannidis, N. M. et al. REVEL: an ensemble method for predicting the pathogenicity of rare missense variants. *Am. J. Hum. Genet* **99**, 877–885 (2016).
24. Livesey, B. J. & Marsh, J. A. Using deep mutational scanning to benchmark variant effect predictors and identify disease mutations. *Mol. Syst. Biol.* **16**, e9380 (2020).
25. Raimondi, D. et al. DEOGEN2: prediction and interactive visualization of single amino acid variant deleteriousness in human proteins. *Nucleic Acids Res.* **45**, W201–W206 (2017).
26. Riesselman, A. J., Ingraham, J. B. & Marks, D. S. Deep generative models of genetic variation capture the effects of mutations. *Nat. Methods* **15**, 816–822 (2018).
27. Vaser, R., Adusumalli, S., Leng, S. N., Sikic, M. & Ng, P. C. SIFT missense predictions for genomes. *Nat. Protoc.* **11**, 1–9 (2016).
28. Ley, T. J. et al. *DNMT3A* mutations in acute myeloid leukemia. *N. Engl. J. Med.* **363**, 2424–2433 (2010).

Methods

Participant samples and ethics. This study complies with all relevant ethical regulations. The study protocol was approved by NHS Lothian (formerly Lothian Health). Informed consent was given by all participants. Ethics permission for LBC1936 was obtained from the Multi-Centre Research Ethics Committee for Scotland (wave 1: MREC/01/0/56), the Lothian Research Ethics Committee (wave 1: LREC/2003/2/29) and the Scotland A Research Ethics Committee (waves 2, 3, 4 and 5: 07/MRE00/58). Ethics permission for LBC1921 was obtained from the Lothian Research Ethics Committee (wave 1: LREC/1998/4/183; wave 2: LREC/2003/7/23; wave 3: 1702/98/4/183) and the Scotland A Research Ethics Committee (waves 4 and 5: 10/MRE00/87).

LBC1921 contains a total of 550 participants at wave 1 of their testing (performed between 1999 and 2001) with a gender ratio of 234:316 (male:female) and a mean age at wave 1 of 79.1 years (s.d. = 0.6) (Supplementary Table 1)[17]. LBC1936 contains a total of 1,091 participants at wave 1 of their testing (performed between 2004 and 2007) with a gender ratio of 548:543 (male:female) and a mean age at wave 1 of 69.5 years (s.d. = 0.8) (Supplementary Table 1)[17]. We previously identified 73 participants with CHIP at wave 1 (ref. [18]). We sequenced DNA from those 73 LBC participants using a targeted gene panel (Supplementary Table 8) and added 16 LBC participants with previously unidentified CHIP and 4–5 timepoints. We have accepted 85 of 89 participants for inclusion in our study, removing four participants for failing to meet quality criteria (low library complexity), with a total of 248 samples together with 14 'Genome in a Bottle' (GIAB) controls, two per sequencing batch (Supplementary Table 9)[29]. In addition, two individuals carrying the *JAK2V617F* mutation received treatment for leukemia after the first respective timepoint available, potentially driving the observed reductions in clone size. Those patients were omitted from further analysis after sequencing (Fig. 1h).

Targeted, error-corrected sequencing and data filtering. DNA was extracted from Ethylenediaminetetraacetic acid (EDTA) whole blood using the Nucleon BACC3 kit (Sigma-Aldrich, GERPN8512), following the manufacturer's instructions. Libraries were prepared from 200 ng of each DNA sample using the Archer VariantPlex® 75 Myeloid gene panel and VariantPlex® Somatic Protocol for Illumina sequencing (Invitae, AB0108, and VariantPlex®-HGC Myeloid Kit for Illumina; Supplementary Table 9), including modifications for detecting low allele frequencies. Sequencing of each pool was performed using the NextSeq 500/550 High-Output version 2.5 (300 cycle) kit on the NextSeq 550 platform (Illumina). To inform reproducibility, background model for error and batch correction, we sequenced two GIAB DNA samples in each batch of samples (DNA NA12878, Coriell Institute)[29].

Reads were filtered for phred ≥30 and adapters removed using Trimmomatic (version 0.27)[30] before undergoing guided alignment to human genome assembly hg19 using bwa-mem (version 0.7.17)[31] and bowtie2 (version 2.2.1)[32]. Unique molecular barcodes (ligated before PCR amplification) were used for read de-duplication to support quantitative multiplexed analysis and confident mutation detection. Within targeted regions, variants were called using three tools (Lofreq (version 2.1.0)[33], Freebayes[34] and Vision (ArcherDX version 6.2.7, unpublished)), building a consensus from the output of all callers (Supplementary Table 2).

All filtered variants at 2% VAF met the following criteria: (1) the number of reads supporting the alternative allele surpasses the coverage criteria while exhibiting no directional biases (AO ≥ 5, UAO ≥ 3); (2) variants are significantly underrepresented in the Genome Aggregation Database (gnomAD; $P \leq 0.05$)[35]; (3) variants are not obviously germline variants (stable VAF across all waves ~0.5 or ~1) that may have been underrepresented in the gnomAD due to the narrow geographical origin of the LBC participants; and (4) contain events that are overrepresented across the dataset—generally frameshift duplications and deletions—whose reads share some sequence homology to target regions yet are likely misaligned artifact from the capture method (Supplementary Table 2). In addition, we manually curated this list, checking for variants that were previously reported, as per Jaiswal et al.[5], in COSMIC[20] or in the published literature (Supplementary Table 10). Finally, for any variant that surpassed the above criteria at VAF ≥ 2% across the measured time period, we included other participant-matched data points regardless of VAF level (Extended Data Fig. 1a,b).

To further mitigate against the diverse sources of noise that can occur in any sequencing experiment, which can become especially problematic when attempting to detect variants at low VAFs, the ArcherDX variant-calling platform leverages the pan-dataset coverage levels of each sample and the GIAB controls to establish a position-specific noise profile and, thus, ascertain the limit of detection (LOD) for each variant discovered in our panel. Here, we report two parameters for each variant: (1) the minimal detectable allele fraction (95% MDAF; Extended Data Fig. 1c), which describes the minimum VAF that a variant can be detected in our data, in essence describing the LOD for each event; and (2) the VAF outlier *P* value, which denotes the probability that any variant call could have been generated by sequencing noise given the position-specific noise distribution across our GIAB controls and the pan-dataset coverage levels of our samples, thus allowing us to discern overrepresented sequencing artifacts from real events (Extended Data Fig. 1d).

Computational prediction of missense variant effects. To predict which missense variants are most likely to be damaging, we used seven computational variant effect predictors recently identified as being most useful for identifying pathogenic mutations[21–27]. Specifically, for each variant identified in this study, we determined what fraction of previously identified pathogenic and likely pathogenic missense variants from ClinVar and what fraction of variants observed in the human population from gnomAD version 2.1 for each computational predictor. We then averaged these fractions across all predictors. Note that DeepSequence[26] was not run for all proteins due to its computational intensiveness and difficulty of running on long protein sequences. We also performed predictions of missense variant (de)stabilization using FoldX 5.0, using the experimentally determined protein structure, if available, and the AlphaFold model[36,37].

Mathematical model of clonal dynamics to infer fitness. Given the longitudinal nature of this study, we can use the probabilistic solution of an established minimal model of cell division[14,38] to infer the parameter distribution resulting in the observed time evolution of VAF trajectories in a participant's genetic profile (Fig. 2a). For each individual, we simultaneously estimated the fitness of variants as well as the size of the stem cell pool, without needing to estimate the time of mutation acquisition.

In this model, cells exist in two states: stem cells (SCs) or differentiated cells (DCs). Under the assumption that DCs cannot revert to a SC state, differentiation inevitably leads to cell death and is treated as such. Furthermore, assuming that each SC produces the same amount of fully differentiated blood cells allows a direct comparison between the VAF of a variant as observed in blood samples and the number of SCs forming the genetic clone (clone size). For an individual with a collection of clones $\{c_i\}_{i\in I}$, the VAF evolution in time $v_i(t)$ of a clone c_i corresponds to $v_i(t) = \frac{n_i(t)}{2N(t)}$, where $v_i(t)$ is the VAF of the variant at time t; $n_i(t)$ is the number of SCs carrying the variant; and $N(t)$ corresponds to the total number of diploid HSPCs present in the individual. Finally, we assume that $N(t) = N_w + \sum_{i\in I} n_i(t)$, where N_w is the average number of wild-type HSPCs in the individual. The bias toward self-renewal of symmetric divisions is parameterized by parameter s and determines the fitness advantage of a clone. In normal hematopoiesis, $s = 0$, in which case clones undergo neutral drift. For clones with non-neutral (fitness-increasing) mutations, $s > 0$, and this average clone size grows exponentially in time as $e^{s(t-t_0)}$ from an initial population of one SC at the time of mutation acquisition t_0. The full distribution of clone sizes is well-approximated by a negative binomial distribution matching the mean (exponential growth) and variance of the full stochastic solution (Supplementary Information Methods, section 1, and Extended Data Fig. 4a). Because the model dynamics are Markovian (without memory), once we condition on a previously observed timepoint in a trajectory, the prediction for all future times is independent of t_0. From the predicted clone size distributions, we can infer the marginal posterior distribution of parameter s using Bayes' theorem (Supplementary Information Methods, section 3)[39]. We further take into account the sampling error during sequencing to estimate the distribution of clone sizes at the start and end of each time interval in the longitudinal sequencing data. Here, we approximate this sampling error as binomial.

When multiple fit clones are present in an individual, we constrain the inference to share the SC pool size $N(t)$ for all variant trajectories in this individual. This increases the data:parameter ratio and produces richer dynamics, where the evolution of exponentially growing clones can be suppressed by the growth of a fitter clone. This implies that even non-competitive models, where trajectories grow independently of each other, will result in competitive dynamics in the observed VAF trajectories as variants strive for dominance of the total production of blood cells.

We take into account possible clonal substructures for all fit variants in an individual, selecting models with co-occurring mutations on the same clone if they are more likely after biasing against models with multiple mutations per clone, as these are presumed to be rarer (Supplementary Information Methods, section 2.4.7). The evidence supporting the optimal clonal structure, determined by Bayesian model comparison, relative to the model assuming no mutations co-occur on the same clone is shown in Extended Data Fig. 4d. We then infer the posterior fitness distributions per clone for the most likely clonal model in every participant.

Once we have inferred the posterior distributions of the parameters, we use the mode of the distribution (maximum a posteriori (MAP) estimate) for each mutation to visualize the deterministic—that is, average—growth curves. These result in the logistic time evolution of its corresponding VAF,

$$v(t) = \frac{1}{2 + 2N_w e^{-s(t-t_0)}},$$

where we determine the time of mutation acquisition t_0, which is used only for plotting, using maximum likelihood (Supplementary Information Methods, Appendix B). Although deterministic fits are not a direct reflection of the inference results of our stochastic model, these can be used to visually assess the 'goodness of fit' of the fitness MAP estimates and have been included for each participant in LBC1921 and LBC1936, respectively, in Extended Data Figs. 5 and 6.

Note that this model cannot account for loss-of-heterozygosity events.

LiFT. To select fit variants, we compare the likelihood of the clonal model, including binomial sampling error, to a model of sequencing artifacts. The artifact

model assumes that all variability arises from sampling error with a proportion that remains constant over time. For variants that occur more than once in our dataset, we use a beta-binomial model to account for overdispersion, and, for unique variants, we use a binomial model. We select variants as fit only if the model evidence for the clonal model is at least four times that of the artifact model (Supplementary Information Methods, section 2.4, and Extended Data Fig. 2c,d). Fit variants thus selected are taken through to clonal structure model selection and fitness inference as described above.

Workflow overview. A workflow chart describing the full pipeline and implementation guidance is included in the GitHub repository (see 'Code availability'). Our pipeline can be applied to other datasets with a few adjustments. Our LiFT algorithm has been tailored to the LBC dataset by extracting parameters from the distribution of synonymous mutation reads, which inform the priors used for our Bayesian inference method (Supplementary Information Methods, section 2.3.3, and Extended Data Fig. 2a–c). Guidance on how to adapt our LiFT algorithm to other datasets is included in the code repository. All other parts of the pipeline, including the extraction of variants using ArcherDx software and the inference of clonal structures and fitness, are directly applicable to other datasets.

Framework implementation. Both LiFT and Bayesian inference of the posterior distribution of model parameters were implemented in Python version 3.7 (ref. [40]) with dependencies on Numpy version 1.21.5 (ref. [41]), Scipy version 1.7.3 (ref. [42]) and Pandas version 1.3.4. Survival analysis was implemented using Python version 3.7 (ref. [40]) with dependencies on lifelines version 0.26.4 (ref. [43]). Data curation was undertaken in Python version 3.7 (ref. [40]) and R base[44], with use of the 'tidyverse'[45] suite of packages and plotted with ggplot2 (ref. [46]).

Reporting summary. Further information on research design is available in the Nature Research Reporting Summary linked to this article.

Data availability

We have deposited all data pertinent to this analysis, including the de-identified raw FASTQ read data and processed variant calls for our longitudinal cohort, onto the National Center of Biotechnology Information Gene Expression Omnibus under accession ID GSE178936. LBC phenotypic data are available in the database of Genotypes and Phenotypes (dbGAP) under accession number phs000821.v1.p1. All other Lothian Birth Cohort data are deposited in dbGAP or are provided via the LBC Data Access Collaboration (https://www.ed.ac.uk/lothian-birth-cohorts/data-access-collaboration). Information concerning the cohort is contained here, including its history, data summary tables for both LBC1921 and LBC1936 and data access request forms and contact information to obtain all data points (contact: https://www.ed.ac.uk/profile/simon-cox, simon.cox@ed.ac.uk; timeframe: 1 month to respond).

Code availability

All code used in this manuscript is available at https://github.com/neilrobertson/LBC_ARCHER.

References

29. Zook, J. M. et al. Extensive sequencing of seven human genomes to characterize benchmark reference materials. *Sci. Data* **3**, 160025 (2016).
30. Bolger, A. M., Lohse, M. & Usadel, B. Trimmomatic: a flexible trimmer for Illumina sequence data. *Bioinformatics* **30**, 2114–2120 (2014).
31. Li, H. & Durbin, R. Fast and accurate short read alignment with Burrows–Wheeler transform. *Bioinformatics* **25**, 1754–1760 (2009).
32. Langmead, B., Trapnell, C., Pop, M. & Salzberg, S. L. Ultrafast and memory-efficient alignment of short DNA sequences to the human genome. *Genome Biol.* **10**, R25 (2009).
33. Wilm, A. et al. LoFreq: a sequence-quality aware, ultra-sensitive variant caller for uncovering cell-population heterogeneity from high-throughput sequencing datasets. *Nucleic Acids Res.* **40**, 11189–11201 (2012).
34. Garrison, E. & Marth, G. Haplotype-based variant detection from short-read sequencing. Preprint at https://arxiv.org/abs/1207.3907 (2012).
35. Karczewski, K. J. et al. The mutational constraint spectrum quantified from variation in 141,456 humans. *Nature* **581**, 434–443 (2020).
36. Jumper, J. et al. Highly accurate protein structure prediction with AlphaFold. *Nature* **596**, 583–589 (2021).
37. Varadi, M. et al. AlphaFold Protein Structure Database: massively expanding the structural coverage of protein-sequence space with high-accuracy models. *Nucleic Acids Res.* **50**, D439–D444 (2022).
38. Till, J. E., Mcculloch, E. A. & Siminovitch, L. A stochastic model of stem cell proliferation, based on the growth of spleen colony-forming cells. *Proc. Natl Acad. Sci. USA* **51**, 29–36 (1964).
39. Bayes, T. An essay towards solving a problem in the doctrine of chances. By the late Rev. Mr. Bayes, F. R. S. communicated by Mr. Price, in a letter to John Canton, A. M. F. R. S. https://doi.org/10.1098/rstl.1763.0053 (1763).
40. Van Rossum, G. & Drake, F. L. *Python 3 Reference Manual*. https://dl.acm.org/doi/book/10.5555/1593511 (CreateSpace, 2009).
41. Harris, C. R. et al. Array programming with NumPy. *Nature* **585**, 357–362 (2020).
42. Virtanen, P. et al. SciPy 1.0: fundamental algorithms for scientific computing in Python. *Nat. Methods* **17**, 261–272 (2020).
43. Davidson-Pilon, C. lifelines: survival analysis in Python. *J. Open Source Softw.* **4**, 1317 (2019).
44. R Core Team. R: a language and environment for statistical computing. https://www.R-project.org/ (R Foundation for Statistical Computing, 2021).
45. Wickham, H. et al. Welcome to the tidyverse. *J. Open Source Softw.* **4**, 1686 (2019).
46. Wickham, H. *ggplot2: Elegant Graphics for Data Analysis*. https://ggplot2.tidyverse.org (Springer-Verlag, 2016).

Acknowledgements

We gratefully acknowledge the contributions of the LBC participants and members of the LBC research team who collect and manage the LBC data. We thank C. P. Ponting for critical reading of the manuscript. We would also like to thank B. Tait for his help, advice and patience throughout. LBC1921 was supported by the UK's Biotechnology and Biological Sciences Research Council (BBSRC) (SR176) to I.J.D; by a Royal Society–Wolfson Research Merit Award to I.J.D.; and by the Chief Scientist Office of the Scottish Government's Health Directorates (CZB/4/505; ETM/55) to I.J.D. LBC1936 is supported by the BBSRC and the Economic and Social Research Council (BB/W008793/1) to S.R.C; Age UK (Disconnected Mind project, which supports S.E.H) to I.J.D and S.R.C.; the Medical Research Council (MR/M01311/1 to I.J.D. and MR/K026992/1 to S.R.C.); and the University of Edinburgh. K.K. is funded by a John Goldman Fellowship, sponsored by Leukaemia U.K. (2019/JGF/003 to K.K.) and received CRUK Glasgow Centre funding (C7932/A25142 to K.K.) and CRUK Scotland Centre funding (CTRQQR-2021\100006 to K.K.). M.T.T. and N.A.R. are supported by Medical Research Council-funded Ph.D. studentships (MR/N013166/1 to M.T.T. and N.A.R.). T.C. and L.S. are supported by Chancellor's Fellowships held at the University of Edinburgh. J.A.M. is a Lister Institute Research Prize Fellow. E.L.C. is a cross-disciplinary postdoctoral fellow supported by funding from the University of Edinburgh and the Medical Research Council (MC_UU_00009/2). S.R.C. is supported by a Sir Henry Dale Fellowship, jointly funded by the Wellcome Trust and the Royal Society (221890/Z/20/Z). We are also grateful for funding from the Howat Foundation (grant holder, M.C.).

Author contributions

L.J.S., K.K. and T.C. conceived and supervised the study. N.A.R., E.L.C., L.J.S., K.K. and T.C. wrote the manuscript. L.M., A.F. and L.M.G. generated data. N.A.R. and E.L.C. developed the methodology for data analysis. N.A.R., E.L.C., M.T.T., A.C.P., J.A.M., B.J.L., J.L.P., R.F.H., R.E.M. and J.L.P. conducted data analysis. S.E.H., S.R.C. and I.J.D. curated the LBCs and gave access to samples. M.C. advised on aspects of the study.

Competing interests

K.K. received a reagent grant from ArcherDX/Invitae. L.M. consults for Illumina. M.C. has received research funding from Cyclacel and Incyte, is/has been an advisory board member for Novartis, Incyte, Pfizer and Jazz Pharmaceuticals and has received honoraria from Astellas, Novartis, Incyte, Pfizer and Jazz Pharmaceuticals. The remaining authors declare no competing interests.

Additional information

Extended data is available for this paper at https://doi.org/10.1038/s41591-022-01883-3.

Supplementary information The online version contains supplementary material available at https://doi.org/10.1038/s41591-022-01883-3.

Correspondence and requests for materials should be addressed to Linus J. Schumacher, Kristina Kirschner or Tamir Chandra.

Peer review information *Nature Medicine* thanks Jamie Blundell, Alejo Rodriguez-Fraticelli, Hubert Serve and the other, anonymous, reviewer(s) for their contribution to the peer review of this work. Primary handling editor: Anna Maria Ranzoni, in collaboration with the *Nature Medicine* team.

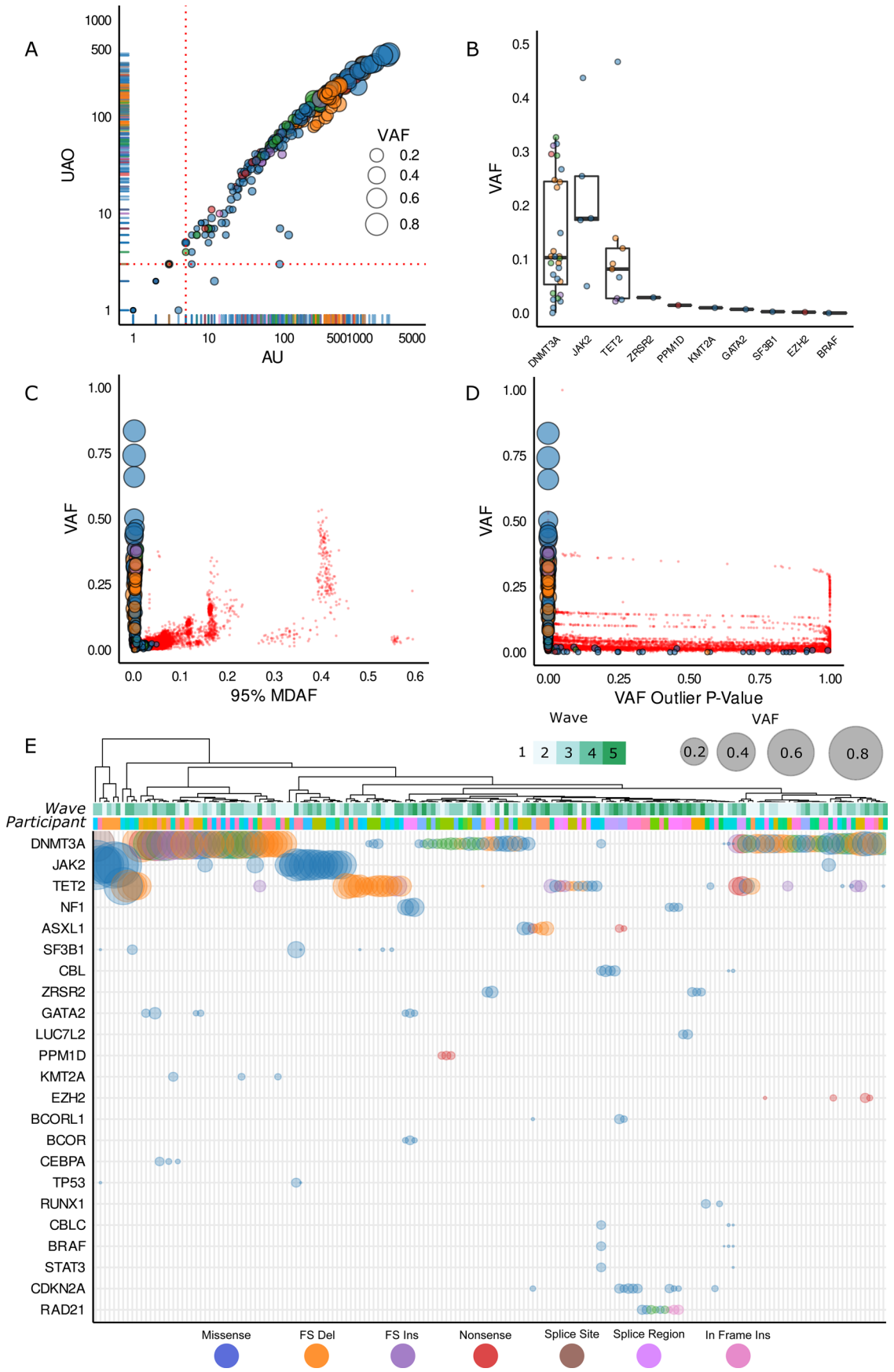

Extended Data Fig. 1 | See next page for caption.

Extended Data Fig. 1 | Quality Control Metrics. a. Sequence quality metrics for mutation calls across participants and time-points filtered for 2% VAF. Plotted are the AO (the number of sequenced reads supporting the alternative allele (mutation)) against the UAO (the number of sequenced reads with unique start sites that support the alternative allele - a measure of molecular complexity). Red dotted lines denote filter thresholds in both measurements ($AO \geq 5$, $UAO \geq 3$) and points are scaled by the VAF of the somatic mutation. Only 7 (of 275) data points failed to meet our filter criteria which were not excluded as they were supported with matching events across any participants' time series. **b**. Box and jitter plot of the variant allele frequency of all observed events in the 1st Wave at 2% VAF coloured by variant classification and ordered by largest mean VAF showing the median and interquartile range. **c**. The 95% MDAF (Minimal Detectable Allele Fraction with 95% Confidence) versus the VAF for each event. All variants used in our analysis above 2% VAF are scaled by their clone size and coloured by their functional consequence. Points in red are events that failed to pass our quality criteria and are removed from subsequent work. **d**. The VAF Outlier P-Value (describing the pan-cohort position-specific background noise) versus VAF for each event. All variants used in the analysis above 2% VAF are scaled by their clone size and coloured by their functional consequence. Points in red are events that failed to pass our quality criteria and are removed from subsequent work. All accepted events that exceed VAF Outlier P-Value > 0.1 are generally low VAF and are supported by matching events across the time-series that adhere to our acceptance criteria of VAF Outlier P-Value ≤ 0.1. **e**. Schematic of all affected genes in the cohort with the largest clone size of an event in any given gene shown above 2% VAF. All affected participants have been clustered across all time-points, with the point size scaled by VAF and coloured by the functional consequence of the variant (as per legend).

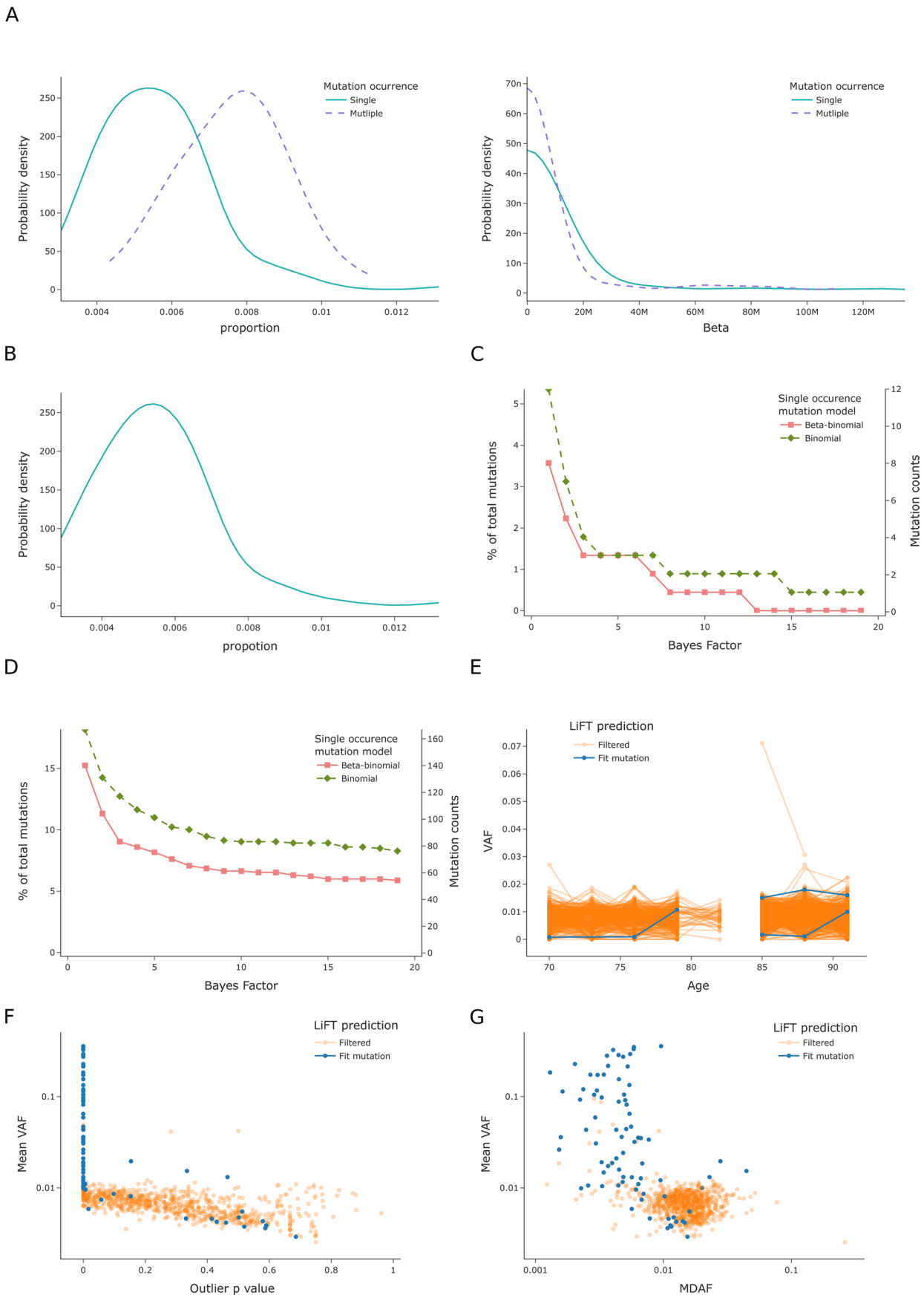

Extended Data Fig. 2 | See next page for caption.

Extended Data Fig. 2 | LiFT Method Details. a. Prior distributions for the beta-binomial model for sequencing artefacts. Priors are constructed separately for mutations with a single occurrence and mutations with multiple observations in the LBCs (see SI methods Section 2.3). **b**. Prior distribution of the proportion for the binomial model for sequencing artefacts. This prior is constructed only for mutations with a single occurrence in the LBC. **c**. Effect of the Bayes Factor (BF) threshold on the number of non-synonymous variants selected as fit using LiFT. In red, we show the results assuming that sequencing artefacts always follow a beta-binomial model, regardless of the mutation occurrence in the LBC. In green, we show the results where the sequencing artefact model assumes a binomial model for single occurring mutations and a beta-binomial model for mutations with multiple occurrences in the LBCs. **d**. Effect of the BF on the number of synonymous variants selected as fit using LiFT. Colour coding as in Fig. S2C. **e**. Longitudinal trajectories of non-synonymous variants coloured by their LiFT status; fit (blue) and filtered (orange). **f**. Comparison between LiFT status and the VAF Outlier P-value. Each data point corresponds to a trajectory in the LBC and has been coloured according to its LiFT status; fit (blue) and filtered (orange). The coordinates of each data point are given by the average VAF Outlier p-Value and their average VAF. **g**. Comparison between LiFT status and the Minimal Detectable Allele Fraction (MDAF). Each data point corresponds to a trajectory in the LBC and has been coloured according to its LiFT status; fit (blue) and filtered (orange). The coordinates of each data point are given by the average MDAF and their average VAF. Note that the MDAF is shown on a logarithmic scale.

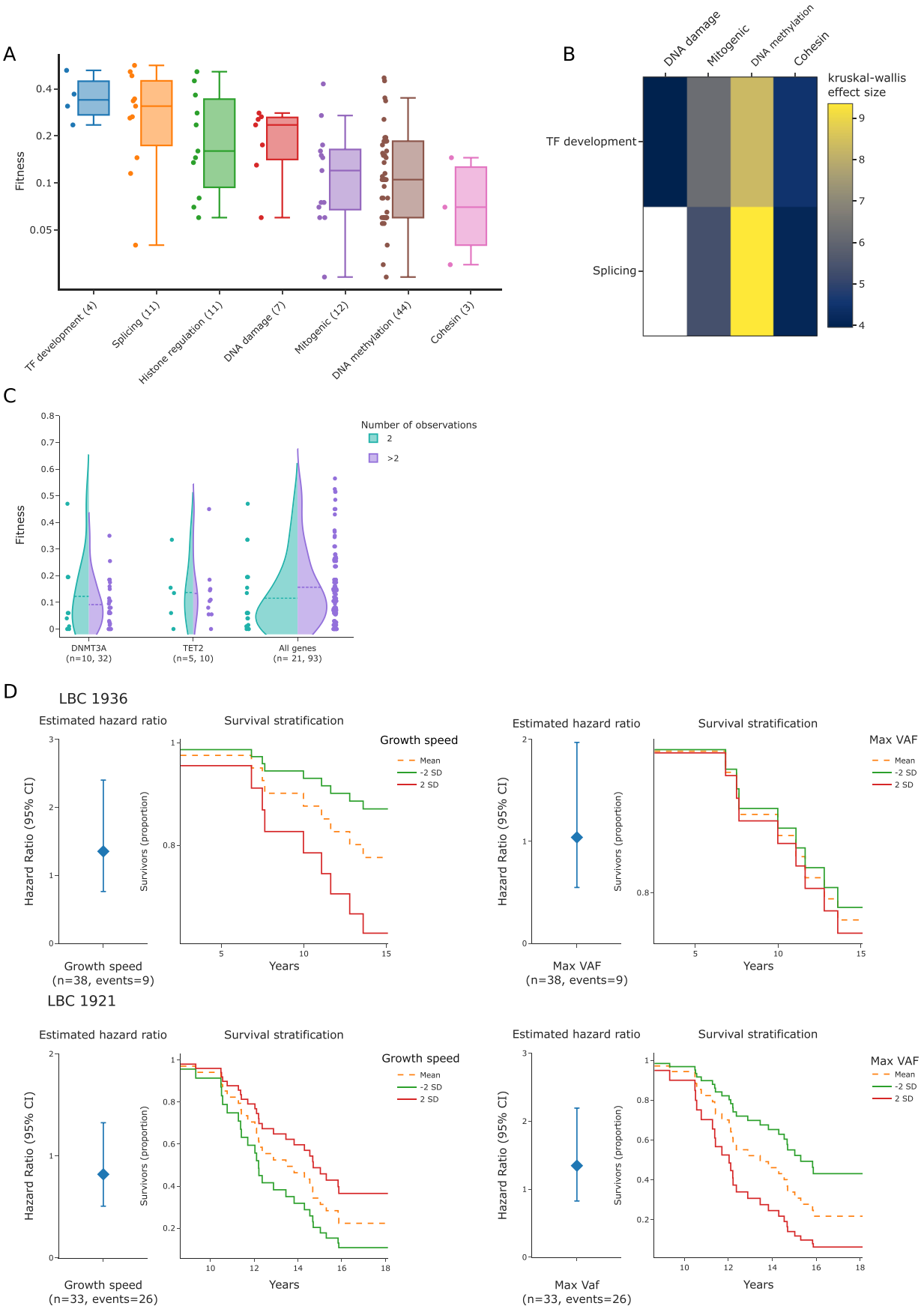

Extended Data Fig. 3 | See next page for caption.

Extended Data Fig. 3 | Clinical Relevance of LiFT - Supporting Material. a. Distribution of fitness by gene category. Genes are grouped according to their biological function into DNA methylation (*TET2, DNMT3A*), Splicing (*SF3B1, U2AF1, SRSF2, U2AF2, ZRSR2, LUC7L2, DDX41*), mitogenic function (*KRAS, NF1, JAK2, JAK3, SH2B3, PTEN, PTPN11, NRAS*), cohesin (*RAD21, STAG2*), DNA damage (*TP53, CDKN2A, PPM1D, ATRX*) and Transcription factors (TF) important during development (*GATA2, RUNX1, NOTCH1, CUX1, ETV6*). The sample size, n, of each gene category is denoted in brackets. For each gene category we display a boxplot showing the maximum a posteriori (MAP) estimates of fitness for variants in the category, as well as the median and exclusive interquartile range. **b**. Analysis of variance of the maximum posterior fitness estimates across gene categories. Heatmap of all statistically significant ($p < 0.05$) Kruskal-Wallis H statistics, labelled by effect size, computed for all combinations of pairs of genes. The effect size is only shown for statistically significant relations. Variants with a fitness below 2% were left out of this study as our prediction classifies them as conferring no or a negligible fitness advantage. **c**. Influence of the number of time-points in a trajectory on the inferred fitness distributions. We show the maximum posterior estimates for genes *DNMT3A* and *TET2* and for all LiFT variants split according to the number of time-points. **d**. Survival analysis (Cox proportional hazards regression model) broken down by cohort and covariates. LBC1921 and LBC1936 are analysed separately given their difference in age during the observed time-span. (left) Error bar showing the inferred hazard ratio coefficient and 95% CI for each regression study, as well as the sample size, n, and the number of observed events in each analysis. Note that none of the survival analyses shown are statistically significant. The complete summary for each analysis is found in Supplementary Table 7. (right) Kaplan-Meyer survival plots for the LBC cohort stratified using 2 standard deviations of the analysed covariate.

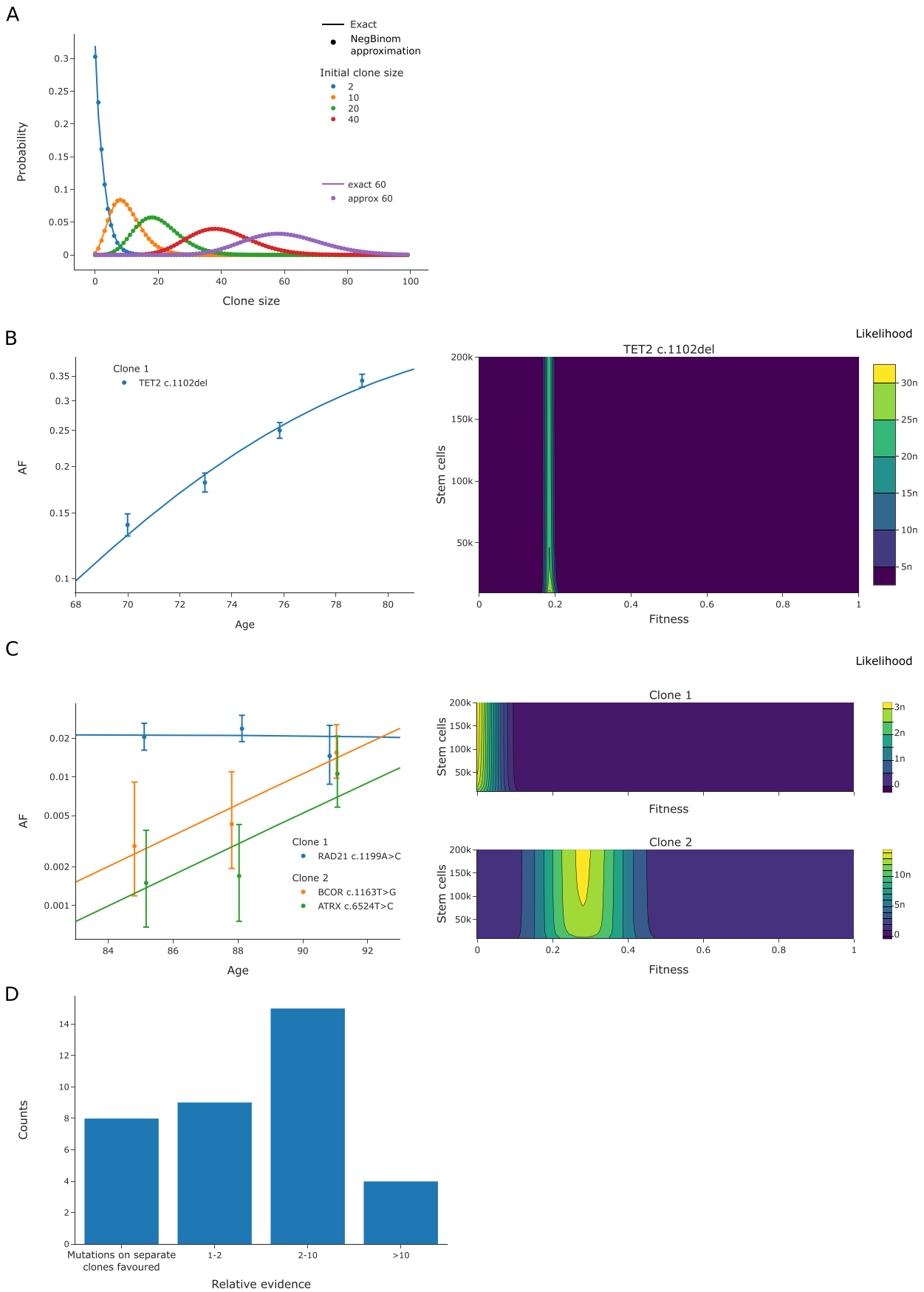

Extended Data Fig. 4 | See next page for caption.

Extended Data Fig. 4 | Clonal Dynamics and Inference - Supporting Material. . **a**. Approximation of a neutral birth-death model using the negative binomial distribution. The exact model assumes symmetric divisions occur every 40 weeks, or 1.3 divisions per year, and has no bias towards self-renewal (see SI methods Section 1). **b**. Deterministic trajectory (see SI methods Appendix B) with maximum a posteriori (MAP) fitness and fitted time of mutation (left) and joint posterior distribution of fitness and number of wild-type HSPCs population (right) inferred from an individual with a single mutation selected by LiFT. 90% confidence intervals associated with binomial sampling noise are shown for each data point. Note that VAF is displayed on a logarithmic scale to highlight relative differences and the initial exponential growth of clones. Also note that a small random horizontal jitter has been added to data points to avoid overlapping of confidence intervals. **c**. Deterministic trajectory (see SI methods Appendix B) with maximum posterior fitness and fitted time of mutation (left) and joint posterior distribution of fitnesses and number of wild-type HSPCs inferred from an individual with three mutations, selected by LiFT, occurring in two clones. 90% confidence intervals associated with binomial sampling noise are shown for each data point. Note that VAF is displayed on a logarithmic scale to highlight relative differences and the initial exponential growth of clones. Also note that a small random horizontal jitter has been added to data points to avoid overlapping of confidence intervals. **d**. Evidence supporting the clonal structure selected by our Bayesian model comparison relative to the model assuming no mutations co-occur on the same clone. The evidence is only shown for non-trivial cases where more than one mutation was selected by LiFT in an individual.

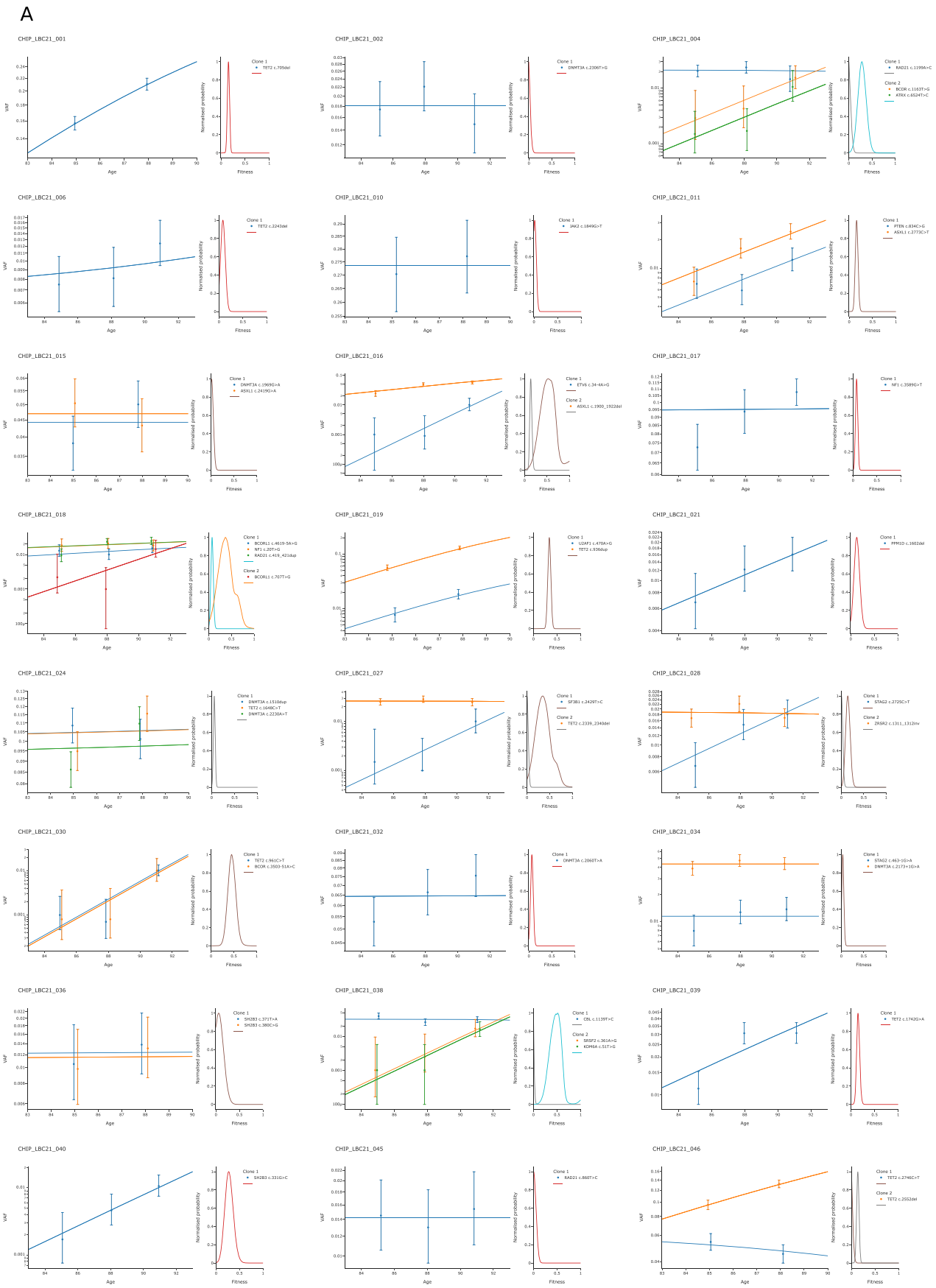

Extended Data Fig. 5 | See next page for caption.

Extended Data Fig. 5 | Deterministic Visualisation of Mutational Trajectories in the LBC21. a. Deterministic trajectories (see SI methods Appendix B) with maximum a posteriori (MAP) fitness and wild-type stem cells and fitted time of mutation (left) and posterior distribution of fitness associated to each clonal structure (right) inferred for all mutations selected by LiFT in each participant of the LBC1921 cohort. 90% confidence intervals associated with binomial sampling noise are shown for each data point. Note that VAF is displayed on a logarithmic scale to highlight relative differences and the initial exponential growth of clones. To use a logarithmic axis, data points with zero observations have been replaced by VAF = 0.001, or a factor of 10 below our observation threshold. Also note that a small random horizontal jitter has been added to data points to avoid overlapping of confidence intervals.

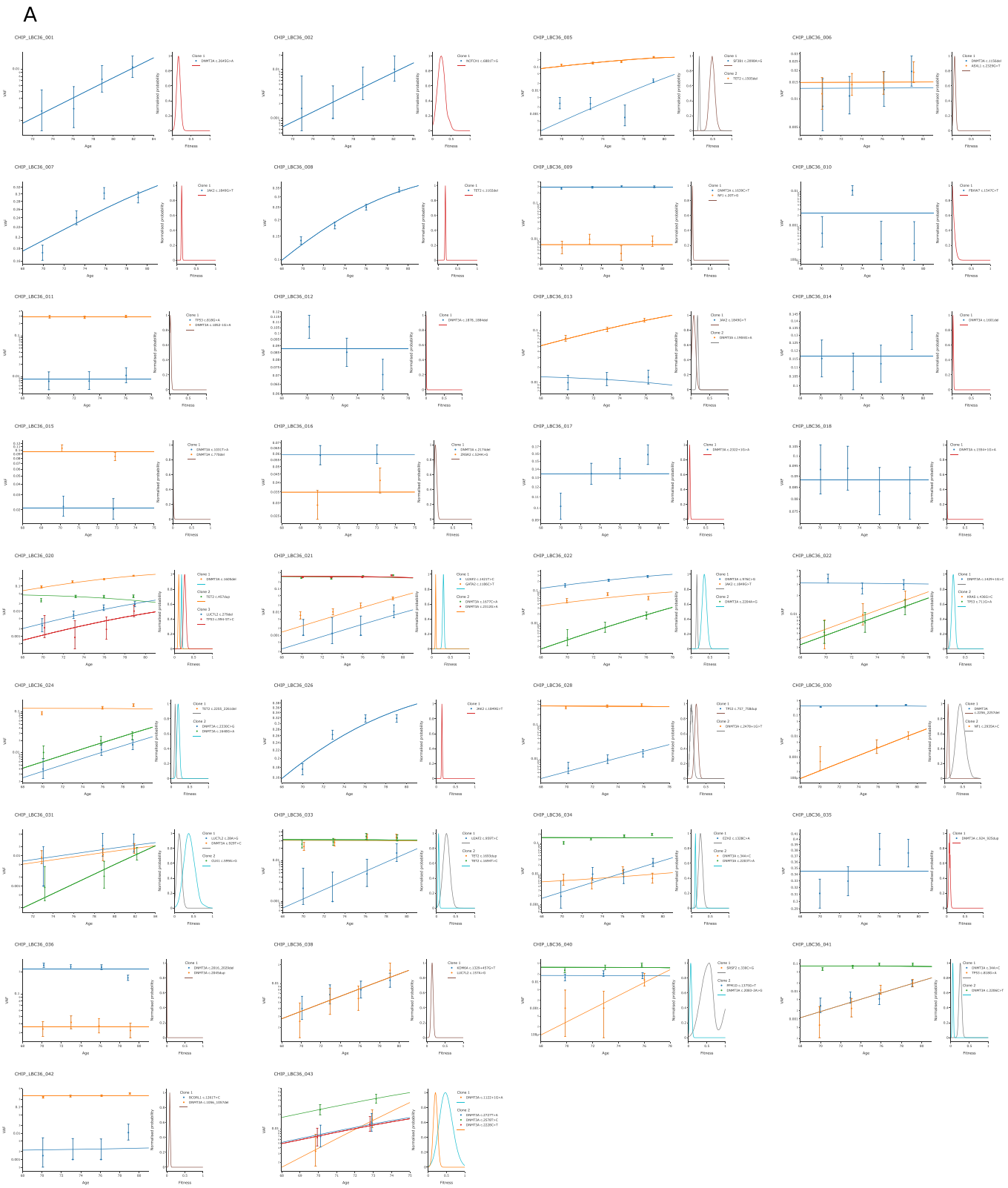

Extended Data Fig. 6 | Deterministic Visualisation of Mutational Trajectories in the LBC36. a. Deterministic trajectories (see SI methods Appendix B) with maximum a posteriori (MAP) fitness and wild-type stem cells and fitted time of mutation (left) and posterior distribution of fitness associated to each clonal structure (right) inferred for all mutations selected by LiFT in each participant of the LBC1936 cohort. 90% confidence intervals associated with binomial sampling noise are shown for each data point. Note that VAF is displayed on a logarithmic scale to highlight relative differences and the initial exponential growth of clones. To use a logarithmic axis, data points with zero observations have been replaced by VAF = 0.001, or a factor of 10 below our observation threshold. Also note that a small random horizontal jitter has been added to data points to avoid overlapping of confidence intervals.

nature research

Corresponding author(s): Linus Schumacher, Kristina Kirschner, Tamir Chandra

Last updated by author(s): Jan 5, 2022

Reporting Summary

Nature Research wishes to improve the reproducibility of the work that we publish. This form provides structure for consistency and transparency in reporting. For further information on Nature Research policies, see our Editorial Policies and the Editorial Policy Checklist.

Statistics

For all statistical analyses, confirm that the following items are present in the figure legend, table legend, main text, or Methods section.

n/a	Confirmed
☐	☒ The exact sample size (*n*) for each experimental group/condition, given as a discrete number and unit of measurement
☒	☐ A statement on whether measurements were taken from distinct samples or whether the same sample was measured repeatedly
☐	☒ The statistical test(s) used AND whether they are one- or two-sided *Only common tests should be described solely by name; describe more complex techniques in the Methods section.*
☐	☒ A description of all covariates tested
☐	☒ A description of any assumptions or corrections, such as tests of normality and adjustment for multiple comparisons
☐	☒ A full description of the statistical parameters including central tendency (e.g. means) or other basic estimates (e.g. regression coefficient) AND variation (e.g. standard deviation) or associated estimates of uncertainty (e.g. confidence intervals)
☐	☒ For null hypothesis testing, the test statistic (e.g. *F*, *t*, *r*) with confidence intervals, effect sizes, degrees of freedom and *P* value noted *Give P values as exact values whenever suitable.*
☐	☒ For Bayesian analysis, information on the choice of priors and Markov chain Monte Carlo settings
☒	☐ For hierarchical and complex designs, identification of the appropriate level for tests and full reporting of outcomes
☐	☒ Estimates of effect sizes (e.g. Cohen's *d*, Pearson's *r*), indicating how they were calculated

Our web collection on statistics for biologists contains articles on many of the points above.

Software and code

Policy information about availability of computer code

Data collection	No software was used for data collection
Data analysis	All the code developed for the data analysis of this article is publicly available and documented in the Github repository: https://github.com/neilrobertson/LBC_ARCHER Workflow overview A workflow chart describing the full pipeline and implementation guidance are included in the github repository (see Code Availability). Our pipeline can be applied to other datasets with a few adjustments. Our LiFT algorithm has been tailored to the LBC dataset by extracting parameters from the distribution of synonymous mutation reads which inform the priors used for our Bayesian inference method (see SI methods Section 2.3.3 and Extended Data Fig. A, B and C). Guidance on how to adapt our LiFT algorithm to other datasets is included in the code repository. All other parts of the pipeline, including the extraction of variants using ArcherDx software and the inference of clonal structures and fitness, are directly applicable to other datasets. Data analysis is split in 3 parts: 1) Variant calling, data aggregation and quality control * Variant calling and raw data processing was completed using the ArcherDX/Invitea analysis pipeline. This was received as a virtual machine that was hosted within the University of Edinburgh (Virtualisation Team). https://analysis.archerdx.com/static/Archer_Analysis_Manual_4_1_0.pdf * Data aggregation was performed using python and R scripts contained in a sub-folder within the Git repository. Data curation was undertaken in Python v.3.7 and R base with use of the "tidyverse" suite of packages and plotted with ggplot2.

2) Longitudinal analysis of variants.
Longitudinal analysis of variants is implemented in Python v.3.7 with dependencies on Numpy v.1.21.5, Scipy v.1.7.3 and Pandas 1.3.4.
Survival analysis was implemented using Python v.3.7 with dependencies on Lifelines 0.26.4.

3) Survival analysis.
Survival analysis is implemented in Python programming language using Lifelines package.

For manuscripts utilizing custom algorithms or software that are central to the research but not yet described in published literature, software must be made available to editors and reviewers. We strongly encourage code deposition in a community repository (e.g. GitHub). See the Nature Research guidelines for submitting code & software for further information.

Data

Policy information about availability of data

All manuscripts must include a data availability statement. This statement should provide the following information, where applicable:

- Accession codes, unique identifiers, or web links for publicly available datasets
- A list of figures that have associated raw data
- A description of any restrictions on data availability

We have deposited all data pertinent to this analysis including the de-identified raw fastq read data and processed variant calls for our longitudinal cohort onto the NCBI Gene Expression Omnibus (Geo) with accession ID: GSE178936 (https://www.ncbi.nlm.nih.gov/geo/query/acc.cgi?acc=GSE178936). LBC phenotypic data are available at dbGAP under the accession number phs000821.v1.p1 (https://www.ncbi.nlm.nih.gov/projects/gap/cgi-bin/study.cgi?study_id=phs000821.v1.p1).

All other Lothian Birth Cohort Data are deposited in dbGAP or provided via the LBC DAC (https://www.ed.ac.uk/lothian-birth-cohorts/data-access-collaboration). Information concerning the cohort is contained here: including its history, data summary tables for both LBC1921 and LBC1936 with data access request forms and contact information to obtain all data points.

Field-specific reporting

Please select the one below that is the best fit for your research. If you are not sure, read the appropriate sections before making your selection.

☒ Life sciences ☐ Behavioural & social sciences ☐ Ecological, evolutionary & environmental sciences

For a reference copy of the document with all sections, see nature.com/documents/nr-reporting-summary-flat.pdf

Life sciences study design

All studies must disclose on these points even when the disclosure is negative.

Sample size	Sample size was not estimated but samples were selected on the basis of harbouring CHIP variants in previous whole genome sequencing (WGS) at wave one. Our methodology is designed to determine fitness estimates in single samples, ergo, sample size was deemed sufficient.
Data exclusions	The study was initially focused on healthy cognitive ageing; at the inception of the study (at approximately age 70), participants were recruited if they reported no dementia or other neurodegenerative diagnoses. In addition, to take part in the first wave of the study, participants had to have been born in 1936 in Scotland, and be living in the Edinburgh and Lothians area of Scotland when recruited. Some data-points
Replication	not applicable
Randomization	not applicable
Blinding	not applicable

Reporting for specific materials, systems and methods

We require information from authors about some types of materials, experimental systems and methods used in many studies. Here, indicate whether each material, system or method listed is relevant to your study. If you are not sure if a list item applies to your research, read the appropriate section before selecting a response.

Materials & experimental systems

n/a	Involved in the study
☒	☐ Antibodies
☒	☐ Eukaryotic cell lines
☒	☐ Palaeontology and archaeology
☒	☐ Animals and other organisms
☐	☒ Human research participants
☒	☐ Clinical data
☒	☐ Dual use research of concern

Methods

n/a	Involved in the study
☒	☐ ChIP-seq
☒	☐ Flow cytometry
☒	☐ MRI-based neuroimaging

Human research participants

Policy information about studies involving human research participants

Population characteristics	The Lothian Birth Cohort 1921 (LBC1921) contains a total of 550 healthy participants at Wave 1 of their testing (done between 1999 and 2001) with a gender ratio of 234/316 (m/f) and a mean age at Wave 1 of 79.1 (SD=0.6). The Lothian Birth Cohort 1936 (LBC1936), contains a total of 1091 healthy participants at Wave1 of their testing (done between 2004 and 2007) with a gender ratio of 548/543 (m/f) and a mean age at Wave 1 of 69.5 (SD=0.8) (Taylor et al., 2018)). Both cohorts are Scottish cohorts. Participant characteristics of the whole cohort are described in the articles cited in the box directly below. Participants characteristics of the specific subsample used in the present study are described in the Methods section of the manuscript. There is known range restriction among members of LBC1921 and LBC1936. They were healthier and better educated than members of the general population of the same age, e.g. Johnson et al 2011 Health Psychology 30:1-11.
Recruitment	Recruitment for LBC1921 was similar to LBC1936. The Lothian Birth Cohort 1921 participants were identified for invitation to participate via newspaper advertisements and also via linkage with the NHS to identify addresses of those individuals born in 1921 living in the region (most schoolchildren in 1932 had taken the Scottish Mental Survey 1932 at school, and the study was designed as a follow-up of those older adults, aged ~79 at recruitment). The Lothian Birth Cohort 1936 participants were identified for invitation to participate via newspaper advertisements and also via linkage with the NHS to identify addresses of those individuals born in 1936 living in the region (most schoolchildren in 1936 had taken the Scottish Mental Survey 1947 at school, and the study was designed as a follow-up of those older adults, aged ~70 at recruitment. The study protocol papers that describe this recruitment process - along with the ethical approvals - are described in detail in the following open access protocol papers: https://www.ncbi.nlm.nih.gov/pmc/articles/PMC2222601/ https://pubmed.ncbi.nlm.nih.gov/22253310/ https://www.ncbi.nlm.nih.gov/pmc/articles/PMC6124629/
Ethics oversight	Ethics permission for the Lothian Birth Cohort 1936 was obtained from the Multi-Centre Research Ethics Committee for Scotland (Wave 1: MREC/01/0/56), the Lothian Research Ethics Committee (Wave 1: LREC/2003/2/29), and the Scotland A Research Ethics Committee (Waves 2, 3, 4 & 5: 07/MRE00/58). Ethics permission for the Lothian Birth Cohort 1921 (LBC1921) was obtained from the Lothian Research Ethics Committee (Wave 1: LREC/1998/4/183; Wave 2: LREC/2003/7/23; Wave 3: 1702/98/4/183) and the Scotland A Research Ethics Committee (Waves 4 and 5: 10/MRE00/87).

Note that full information on the approval of the study protocol must also be provided in the manuscript.